Computers, Materials & Continua

Tech Science Press

Doi:10.32604/cmc.2025.070422

ARTICLE

A Lightweight Multimodal Deep Fusion Network for Face Antis Poofing with Cross-Axial Attention and Deep Reinforcement Learning Technique

Diyar Wirya Omar Ameenulhakeem* **and Osman Nuri Uçan**

School of Engineering and Natural Sciences, Electrical and Computer Engineering, Altınbaş University, Istanbul, 34218, Türkiye

*Corresponding Author: Diyar Wirya Omar Ameenulhakeem. Email: 213720196@ogr.altinbas.edu.tr

Received: 16 July 2025; Accepted: 22 August 2025; Published: 23 October 2025

ABSTRACT: Face antispoofing has received a lot of attention because it plays a role in strengthening the security of face recognition systems. Face recognition is commonly used for authentication in surveillance applications. However, attackers try to compromise these systems by using spoofing techniques such as using photos or videos of users to gain access to services or information. Many existing methods for face spoofing face difficulties when dealing with new scenarios, especially when there are variations in background, lighting, and other environmental factors. Recent advancements in deep learning with multi-modality methods have shown their effectiveness in face antispoofing, surpassing single-modal methods. However, these approaches often generate several features that can lead to issues with data dimensionality. In this study, we introduce a multimodal deep fusion network for face anti-spoofing that incorporates cross-axial attention and deep reinforcement learning techniques. This network operates at three patch levels and analyzes images from modalities (RGB, IR, and depth). Initially, our design includes an axial attention network (XANet) model that extracts deeply hidden features from multimodal images. Further, we use a bidirectional fusion technique that pays attention to both directions to combine features from each mode effectively. We further improve feature optimization by using the Enhanced Pity Beetle Optimization (EPBO) algorithm, which selects the features to address data dimensionality problems. Moreover, our proposed model employs a hybrid federated reinforcement learning (FDDRL) approach to detect and classify face anti-spoofing, achieving a more optimal tradeoff between detection rates and false positive rates. We evaluated the proposed approach on publicly available datasets, including CASIA-SURF and GREATFASD-S, and realized 98.985% and 97.956% classification accuracy, respectively. In addition, the current method outperforms other state-of-the-art methods in terms of precision, recall, and F-measures. Overall, the developed methodology boosts the effectiveness of our model in detecting various types of spoofing attempts.

KEYWORDS: Face antispoofing; lightweight; multimodal; deep feature fusion; feature extraction; feature optimization

1 Introduction

With the widespread use of face recognition technology in smartphones, online authentication systems, and smart surveillance, secure and reliable identity verification has become more important [1]. Although face recognition systems are convenient and accurate, they are vulnerable to various presentation attacks such as printed photos, playback videos, 3D silicone masks, paper faces, or even AI-generated DeepFakes [2]. To address these threats, the field of Face AntiSpoofing (FAS) has developed with the goal of detecting and preventing presentation attacks for facial recognition systems [3]. FAS aims to separate real faces from spoof attempts, making it crucial for biometric security, where malicious and illegitimate access is detected prior to authentication [4].

In recent years, researchers have developed numerous deep learning techniques for designing reliable and robust FAS systems [5–8]. These techniques typically utilize Convolutional Neural Networks (CNNs), supplemented with attention-based optimization techniques, to separate real faces from spoofed faces. While these techniques have demonstrated good results on controlled, within-dataset evaluations, their generalization across various spoof types and unseen domains continues to pose a major challenge. One of the main problems arises from the global attention mechanisms used in these methods, which add computational expense and generally disregard the local discriminative cues that are useful for detecting small spoof artifacts [9]. As a result, prediction consistency for models currently implemented in this context may not be sustained in real-world, cross-dataset applications.

An additional limitation of current deep learning-based FAS systems is that they are reliant on entangled feature representations that conflate identity, illumination, and spoof-related cues within the feature space learned by the model [10]. This entanglement not only affects classifier performance but also diminishes interpretability. While recent attempts have been made to disentangle this feature representation or use attention models that focus on spoof-relevant areas, they either require additional identity labels (which may not always be available) or global attention plans that are not computationally feasible for online use or high-resolution inputs. Moreover, static attention mechanisms are not catered to learning dynamically and are unable to identify significant areas across variable forms of spoofing. Another significant limitation of these methods is the centralization of training, which creates serious privacy issues and restricts deployment in edge or mobile environments. Centralized learning not only introduces additional communication overhead but also fails to deal with the data heterogeneity of client devices and their computational limitations. Although federated learning has been introduced as a privacy-preserving alternative, most federated FAS systems lack intelligent decision-making and adaptive learning capabilities under non-IID data settings.

Motivated by these limitations, we develop a Lightweight Multimodal Deep Fusion Network for FAS, comprising three main modules: Cross-Axial Attention Network (XANet), Enhanced Policy-Based Optimization (EPBO) [11], and Federated Dual-Stage Deep Reinforcement Learning (FDDRL) [12]. Using XANet, we present a structured attention mechanism that captures dependencies across the horizontal and vertical axes independently. Unlike standard global attention mechanisms, which model all spatial interactions simultaneously and thus lead to higher spatial complexity and increased computational overhead, XANet reduces the computational complexity of attention operations from quadratic to linear in spatial dimensions by using axial attention in place of global attention. To further improve the capability for discrimination of the attention modules, the framework incorporates an Enhanced Policy-Based Optimization (EPBO) module. EPBO directly incorporates a Reinforcement Learning (RL) mechanism, whereas experience-based policies can dynamically update attention weights throughout training. It allows the model to selectively emphasize spoof-relevant regions while suppressing noise, improving feature discrimination over time, which results in lower parameter count and improved inference speeds. In addition to these modules, the framework's FDDRL strategy enables privacy-preserving training across distributed client devices while correcting for data imbalance and domain shift through dual-stage optimization.

This step minimizes the client-side computation and communication cost so that it is well-suited for resource-constrained devices. As a results, our proposed model is not only competitive in accuracy, but also lightweight, achieving massively reduced inference latency and memory footprint, allowing for the use of real-time operation on mobile and edge-computing platforms.

The rationale behind this specific combination of XANet, EPBO, and FDDRL lies in their complementary strengths. XANet offered a lightweight yet effective way of capturing structured spatial relationships. EPBO provides an adaptive form of control, making attentional learning more robust against different spoofing cues. FDDRL provides a mechanism that can generate a model for our application that is

constrained for edge-deployment and privacy while improving generalization. Our method combines these previously uncoordinated approaches into a unified architecture that aims to satisfy the multiple constraints of real-world FAS. Further, a hybrid FDDRL-based classification approach discriminated the class-wise optimized features, and performance was compared with eight recently published state-of-the-art art-models: (1) Residual Network (ResNet) [13], (2) Squeeze-and-Excitation Networks (SE-Net) [14], (3) FaceBagNet [15], (4) VisionLabs [16], (5) depthwise separable attention module (DAM) with the multimodal-based feature augment module (MFAM) [17], (6) Masked Frequency Autoencoder [18], (7) M^3FAS [19], and (8) Multiattention-net [20]. The key contributions of the proposed approach are recapitulated below:

1. In the initial phase, we leverage the aXial Attention network model to extract deep hidden features from multimodal images, enhancing the system's ability to discern genuine faces from spoof attempts.
2. Following the feature extraction stage, we employ a bidirectional fusion technique. It pays attention to both directions, facilitating the effective combination of features from each mode. This bidirectional fusion approach contributes to a more comprehensive representation of the input data.
3. Feature optimization is further refined using the EPBO algorithm. It is used to address data dimensionality challenges by selecting and optimizing features, ensuring efficiency in handling complex and high-dimensional data.
4. The proposed model adopts a hybrid federated reinforcement learning approach for the final stages of face antispoofing. This hybrid methodology optimizes the tradeoff between detection rates and false positive rates, enhancing the overall performance of the system. The reinforcement learning aspect contributes to adaptive learning and decision-making, making the model more robust against diverse antispoofing scenarios.

The rest of this paper is organized as follows. Section 1 discusses the review of recent work on face anti-spoofing using deep learning. Section 2 focused on the problem discussion and system architecture of the proposed approach. Section 3 introduces the proposed face antispoofing approach using XANet+EPBO+FDDRL. Section 4 provides experiments and a discussion of the results of the proposed method. Finally, Section 5 concludes this paper.

2 Related Work

Researchers have used a variety of deep learning techniques such as CNNs, attention mechanisms, and training paradigms to build strong, generalizable FAS systems (Table 1). In this section, we review a few recently developed FAS architectures based on CNNs, attention-guided feature learning, and federated learning approaches for privacy-preserving deployment. These studies highlight various advantages to the FAS literature but reveal common challenges related to generalization, interpretability, and operational efficiency. For example, Fatemifar et al. (2021) [21] proposed an FAS system that utilized a fusion-based approach with Weighted Averaging (WA) with a client-specific design and optimized it using two sequential feline Particle Swarm Optimization (PSO) and Pattern Search methods. This system was validated on the Replay-Attack dataset [22], Replay-Mobile dataset [23], and the Rose-Youtu dataset [24], and its performance with these datasets surpassed many other state-of-the-art methods. However, due to the multi-step optimization, this approach may be associated with increased computational expense, making it less applicable to real-time scenarios. Sedik et al. (2022) [25] proposed a deep learning framework using two different architectures, (1) a CNN-based model and (2) a ConvLSTM-based model, to detect face spoofing in videos. The CNN model extracts spatial features from the video frames, whereas the ConvLSTM model can capture spatiotemporal features and fuse them for better representations. Both methods included a fully-connected layer on top of the CNN or ConvLSTM feature layers and subsequently classified them with a SoftMax layer. The ConvLSTM model outperformed classical techniques on the FRAUD1 and FRAUD2 [26] datasets in terms of accuracy,

precision, recall, and Area Under the Curve (AUC). However, as the ConvLSTM combines both temporal and spatial features, this can impact the inference time and reliability in latency-sensitive applications.

Table 1: Summary of related works on face-antispoofing

Reference	Modalities	Approach	Datasets	Limitations
Fatemifar et al. (2021) [21]	RGB	• Fusion with Weighted Averaging Optimized via feline PSO and Pattern Search	• Replay-Attack, • Replay-Mobile, Rose-Youtu	• Multi-step optimization increases computational expense • Not suitable for real-time scenarios
Sedik et al. (2022) [25]	Video (RGB)	• CNN for spatial + ConvLSTM for spatiotemporal fusion	• FRAUD1, • FRAUD2	• Slower inference due to temporal modeling • Less suited for latency-sensitive applications
Kong et al. (2022) [27]	RGB	• Residual network with channel attention • Adaptive weighting of residual features	• Replay-Attack, • CASIA-FASD	• Fixed spatial attention; • Poor generalization to unseen spoofing types and real-world conditions
Huang and Wang (2023) [28]	RGB	• End-to-end FAS with anti-interference • Feature distillation and pyramid binary supervision	• SiW, • OULU-NPU, • CASIA-FASD, • MSU-MFSD, • Replay-Attack	• No explicit mention of generalization across diverse modalities; • Architectural complexity
Xue et al. (2023) [33]	RGB, Depth, IR	• MMSA + Patch Cross Attention for multi-modal fusion	• OULU-NPU, • CASIA-FASD, • Replay-Attack, • CASIA-SURF, • CeFa, • WMCA	• High computational cost due to multiple attention modules Limited suitability for real-time or embedded systems

(Continued)

Table 1 (continued)

Reference	Modalities	Approach	Datasets	Limitations
Yu et al. (2024) [37]	RGB, Depth, IR	• ViT with Adaptive Multimodal Adapter Modality-asymmetric MAE	• WMCA, • CASIA-SURF	• High resource requirements for ViT Challenging for lightweight or real-time applications
Gautam et al. (2024) [38]	RGB, Video	• Federated learning with Canonical Correlation Analysis (CCA) feature fusion	• FaceForensics++, • DeepForensic-1.0, • WildDeepfake	• High computational complexity due to dual CNN usage Unsuitable for real-time applications
Li et al. (2025) [43]	RGB	• CNN with Dual-path Adaptive Channel Attention • Inner Similarity Estimation constraint	• CASIA-SURF, • CeFA, • CASIA-FASD	• Performance may drop in cases of extreme domain shift
Chen et al. (2025) [44]	RGB, Depth, IR	• mmFAS with contrastive-based alignment and switch-attention fusion	• MmFA, • CeFa, • WMCA, • HQ-WMCA	• Training overhead; Requires careful tuning to handle unseen modality shifts.

Kong et al. (2022) [27] presented an FAS scheme that incorporated a residual network and channel attention. The newly proposed scheme highlighted the observed differences in texture, shadow, and edge in the nasal and cheek Area and found adaptive weights according to discriminative residual features. Testing of the model was done on Replay-attack and CASIA-FASD, and was 99.98% and 97.75%. However, its dependency on fixed spatial attention and lack of diversity of different non-forensic spoofing types limit the generalization of the model to unseen spoofing types and real-world conditions. Huang and Wang (2023) [28] presented an end-to-end FAS approach leveraging anti-interference feature distillation and global spatial attention with pyramid binary mask supervision. They had a model that refined multilevel features from ResNet-34 to obtain a more discriminative representation and improve the detection of spoof. The model outperforms the benchmarks using five datasets: SiW [29], OULU-NPU [30], CASIA-FASD [31], MSU-MFSD [32], and Replay-Attack [22] in both a cross- and intra-testing situation.

Xue et al. (2023) [33] developed a hierarchical and multimodal cross-attention model for face anti-spoofing that can be designed for both static (i.e., single modal) and dynamic (i.e., multimodal) inputs. They integrated Multimodal Multihead Self-Attention (MMSA) with Patch Cross Attention (MPCA) to better fuse features obtained across modalities. Experimental results on six public datasets: OULU-NPU [30], CASIA-FASD [31], Replay-Attack [22], CASIA-SURF [34], CASIA-SURF CeFa [35], and WMCA [36] indicate that the model is effective at managing different types of spoofing attacks. However, exploring multiple attention modules for processing input signals adds significant computational costs for the embedding and can lead to limited use of the model in real-time applications. Yu et al. (2024) [37] examined the effects of various inputs, pre-training, and fine-tuning modalities in Vision Transformers (ViT) for multimodal FAS using RGB, Depth, and IR. They report that local descriptors improve ViT on IR but not on RGB or Depth, and that ImageNet pretraining is ineffective in multimodal FAS. To fill these gaps, the authors proposed an Adaptive Multimodal Adapter (AMA) and a modality-asymmetric masked autoencoder (MAE) for efficient self-supervised pretraining. This approach performed better than previous work on WMCA and CASIA-SURF datasets. However, they acknowledge that the inherent resource requirements of ViT may create challenges when deployed in a lightweight or real-time setting.

Gautam et al. (2024) [38] integrated federated learning with their deep learning framework to determine forgery in images and videos. They employed Canonical Correlation Analysis (CCA) [39] to fuse the features extracted from Inception and Xception networks. This approach was trained on three different benchmark forensic data sets (FaceForensics++ [40], Deepforensic-1.0 [41], and WildDeepfake [42]), and achieved superior accuracy in identifying manipulated content. The primary limitation of this approach is its reliance on a complex feature extraction process involving two CNNs, which increases computational cost and makes it unsuitable for real-time applications. Li et al. (2025) [43] presented a CNN-based FAS method that utilized a Dual-path Adaptive Channel Attention (DACA) module to extract facial features and diminish non-relevant information. They introduced an inner similarity estimation (ISE)-based constraint to enforce intra-class compactness while also improving inter-class separability. Experiments performed on the CASIA-SURF, CeFA, and CASIA-FASD datasets show strong performance in differentiating live from spoofed faces. Because of major dependencies on class-specific feature distributions, the effectiveness of the method may be limited in extreme domain shift conditions. Chen et al. (2025) [44] proposed a multimodal FAS framework (mmFAS) that explicitly aligns and fuses latent features across modalities. It introduces a contrastive-based alignment module and a switch-attention fusion mechanism to capture complementary information. The model was strongly validated on four datasets: (1) CeFa [35], (2) WMCA [36], and (3) HQ-WMCA [45]. However, dual-level alignment and attention fusion add training overhead, and it is important to tune the network carefully when experiencing unseen modality shifts.

3 Proposed Methodology

The proposed multimodal deep fusion network consists of four steps: (1) Feature extraction using XANet, (2) Feature amalgamation using a bi-directional fusion scheme, (3) Feature optimization using the EPBO algorithm, and (4) Classification using the FDDRL classifier. The working pipeline of our architecture is shown in Fig. 1. A detailed discussion on all the steps is given in subsequent subsections.

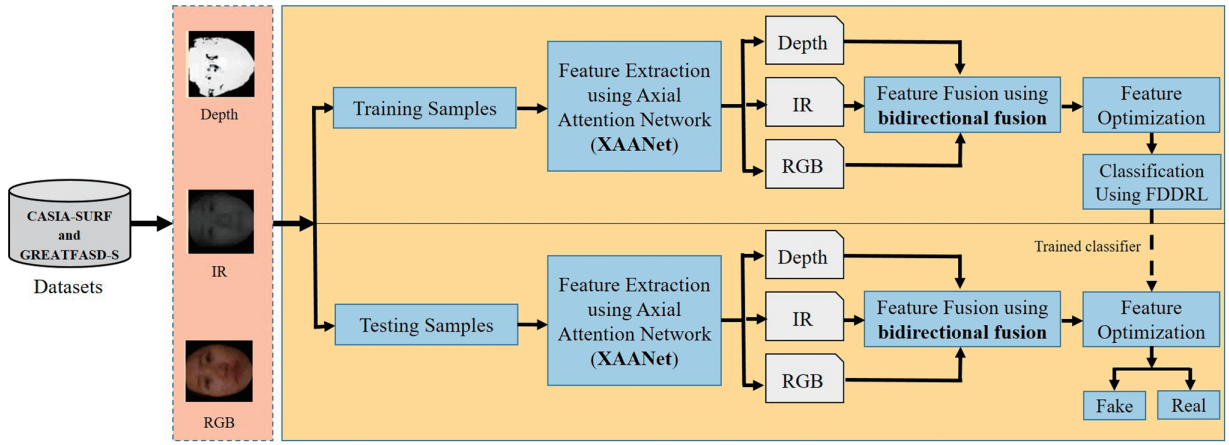

Figure 1: The system architecture of the proposed multimodal deep fusion network

3.1 Feature Extraction

Feature extraction refers to the process of capturing and representing distinctive characteristics or patterns from facial images that are relevant for distinguishing between genuine faces and spoof attempts. This step is crucial for building effective models that can discern the subtle differences between live faces and various presentation attack methods. In our work, we employed both manual and deep features for the characterization of input face scans. Here, four type of manual face imaging attributes: (1) Dimensional attributes (5 features), (2) Facial characteristics (7 features), (3) Image statistics (5 features), and (4) Texture features (4 features) were extracted from all three image modalities (RGB, IR, Depth). Therefore, a total of 63 (21 $*$ 3) features were used for further data processing. The details of all the extracted features from those categories mentioned above are listed in Table 2. Further, a novel XANet was introduced to extract deep features from input facial scans. The details of the developed XANet architecture are introduced in the next subsection.

Table 2: A list of extracted image features from four different categories

Index	Category	Extracted features
1	Dimensional attributes	1. Image Width 2. Image Height 3. Image Length 4. Image Depth 5. Image Shape (Square/Rectangle)
2	Facial characteristics	1. Opacity 2. Eye Color (Brown/Black) 3. Nose Length (Small/Long) 4. Mouth Width (Wide/Medium) 5. Hair Color (Brown/Black) 6. Ear Size (Average/Small) 7. Skin Fair (Fair/Black)

(Continued)

Table 2 (continued)

Index	Category	Extracted features
3	Image statistics	1. Mean_value 2. Standard Deviation 3. Variance 4. Skewness 5. Shannon Entropy
4	Texture features Gray Level Co-occurrence Matrix (GLCM)	1. Contrast Value 2. Energy Value 3. Correlation Value 4. Dissimilarity Value

3.2 Deep Feature Extraction Using XANet Architecture

The primary objective of introducing XANet Architecture is to extract deep features from multimodal facial images. The proposed XANet model is a type of attention-based neural network used in computer vision tasks, particularly for image understanding. Axial attention refers to the mechanism of attending to different axes (rows and columns) of an input tensor separately. The XANet model incorporates this idea to capture long-range dependencies in both the row and column directions of the input data [46]. The proposed network combines a conventional Residual network (RESNet) [13] as a base CNN model with an axial attention mechanism to extract deep face imaging features. It initiates with an Input Layer corresponding to a 32 × 32 RGB image, laying the ground for the next steps. In the Initial Convolution and Pooling phase, a 64-filter Conv2D layer with 7 × 7 kernel size, 2 strides, and 'same' padding is used. Batch Normalization and ReLU activation improve the model's resilience, followed by MaxPool2D with a 3 × 3 kernel, 2 strides, and 'same' padding for spatial subsampling.

The main components of the model are Residual Blocks with Axial Attention. Consisting of four stacks, each containing a certain number of residual blocks, an AxialAttention layer is cunningly embedded in the Middle of each block. Each stack has its number of residual blocks, determined by the num_blocks_list variable, where the value is [2, 2, 2, 2]. The model's capacity increases with every stack, multiplying the number of filters in each block from 64. The Axial Attention Layer (AxialAttention) [47] is a new mechanism, and it combines both row-wise and column-wise axial attention. The row_attention and col_attention layers apply MultiHeadAttention [48] with a key dimension of dim//num_heads. The outputs of these attention mechanisms are also concatenated along the last axis, which gives the model the capability to capture relations along rows and columns separately. The Residual Block (resnet_block) in every stack follows the standard residual architecture. Batch Normalization and ReLU activation follow Conv2D layers of varying filter numbers, 3 × 3 kernel size, and 'same' padding. A shortcut connection is introduced either through a convolutional layer (first block in a stack or first stack) by an addition of the input to the output. Each block is finalized with the ReLU activation layer. The details of the deep feature extraction process are shown in Fig. 2A.

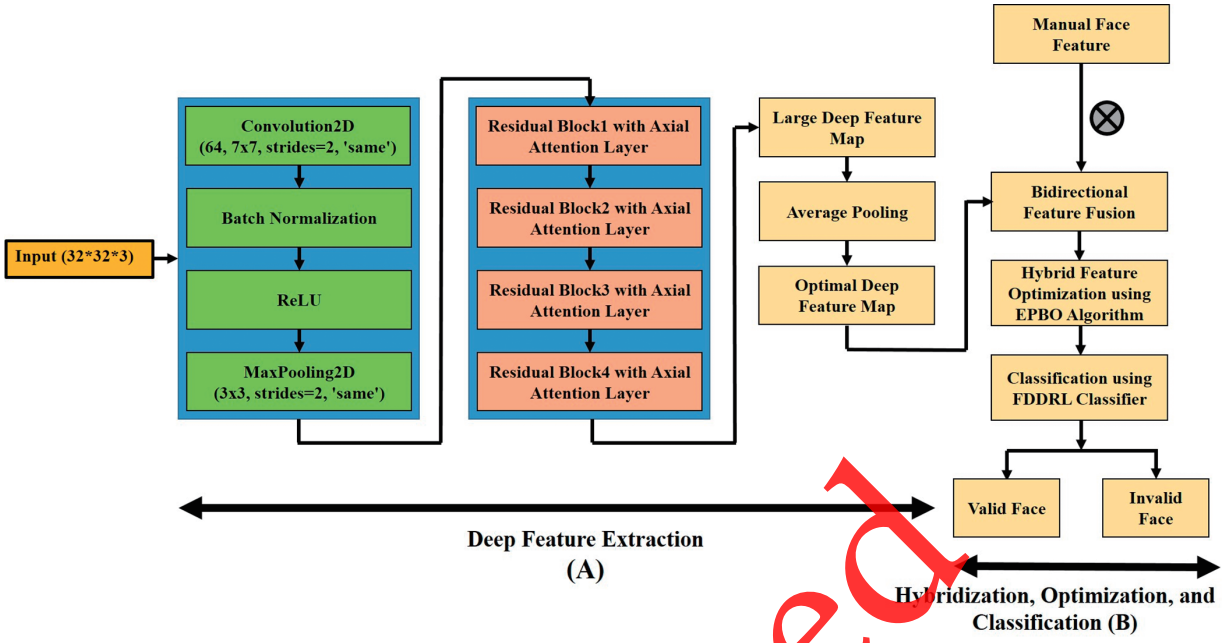

Figure 2: The proposed ant spoofing classification framework. (**A**) Deep feature extraction. (**B**) Hybridization, Optimization, and Classification

3.3 Bidirectional Feature Fusion

In this step, an average pooling procedure was applied to minimize the sparsity level in the deep feature set. The updated features were merged with manual features using a bidirectional feature fusion technique [49]. In this context, bidirectional fusion is applied to combine features from different modes effectively. It captures the reciprocal influence between the modes. This means that the resulting fused features provide a more holistic representation of the input data, capturing both direct and reciprocal relationships. By considering bidirectional information flow, the model potentially captures more complex patterns, dependencies, and interactions between the features of different modes.

3.4 Feature Optimization

Feature optimization typically involves selecting or transforming features in a way that enhances their relevance, discriminative power, or effectiveness for a particular task. In this context, it refers to improving the features extracted from different modes to serve the face antispoofing task better. Here, we introduce the enhanced pity beetle optimization (EPBO) algorithm for feature optimization, which selects the features to address data dimensionality problems. The EPBO algorithm is inspired by the conventional beetle swarm optimization (BSO) [50]. A group of potential solutions called particles is initially scattered in a hypervolume that spans the entire global search space. Here, optimal feature subsets are considered as potential solutions. The particle population is initialized according to the defined search area as follows:

$$q^{(0)} = \left[q_1^{(0)}, q_2^{(0)}, \ldots, q_{B_{pop}}^{(0)}\right]^S \tag{1}$$

$q_g^{(0)}$ represents the optimal features are randomly located in the C-dimensional search space.

$$q_g^{(0)} = rst\left(B_{pop},\ C, L, U\right) \tag{2}$$

here, *rst* is shorthand for an arbitrary search mechanism, which is used to solve the real-time assembly problem. With this first method, all sections of the investigation space are properly considered in the B_{pop} experiments. Where L and U are the best and worst solutions from the initial population. After initialization, fitness is calculated for each solution.

$$f_g(s) = \max \begin{cases} of_1 \\ of_2 \\ of_3 \end{cases} \tag{3}$$

Iteration refers $f_g(s)$ to fitting the g-th solution to s. The solution with maximum fitness is selected as the optimal solution. For each instance, the value of this region is implemented using an appropriately chosen model component (F_x) and EPBO parameterization. According to each example, B_{pop} new precursor particles are computed as follows.

$$q_g^{(j)} = rst\left(B_{pop},\ C, L^{(j)}, U^{(j)}\right) \tag{4}$$

$$\left[l_h^{(j)},\ u_h^{(j)}\right] \in \left[q_{birth,h}^{(j)} * (1 - F_x),\ q_{borth,h}^{(j)} * (1 + F_x)\right] \tag{5}$$

where j represents the generation or next step and $q_{birth,h}^{(j)}$ the h^{th} generation represents the solution vector. $l_h^{(j)}$ and $u_h^{(j)}$ denote the lower and upper bounds of the h^{th} solution for the j^{th} next state, respectively. The neighborhood variable (F_{be}) used to describe the size of this space is the EPBO parameter, OFF_{be} whose value is proportional to the scale [0.01, 0.20]. As this model shows, B_{pop} new precursor particles are generated subjectively and message-dependently on this hunting ground, where F_x is equivalent to F_{be}.

$$q_g^{(0)} = rst\left(B_{pop},\ C, \left[q_{birth,h}^{(j)} * (1 - F_{be}),\ q_{borth,h}^{(j)} * (1 + F_{be})\right]\right) \tag{6}$$

These recent characterization B_{pop} solutions are then interpolated to characterize the ideal precursor molecule. The best is different from the early stage, if the best attracts the best and seeks the newest people:

$$q_{birth,h}^{(j+1)} = \begin{cases} q_{birth,h}^{(j)}, & if\ f\left(q_{birth,h}^{(j)}\right) < \left(q_{g,K}^{(j)}\right) \forall g = 1, 2, \ldots, B_{pop},\ K = 1, 2, \ldots, B_{broods} \\ q_{g,K}^{(j)}, & otherwise \end{cases} \tag{7}$$

A new state $q_{birth,h}^{(j+1)}$ vector is represented in the Kth population, representing B_{broods} the last maximum relatives. The mean scale factor (F_{ae}) used to express the size of this zone is an EPBO parameter whose value corresponds F_{ae} to the scale [0.10, 1.00]. According to this model, B_{pop} recent progenitor particles are located indiscriminately in this hunting cosmic object. where F_x is equal to F_{ae}

$$q_{g,K}^{(j)} = rst\left(B_{pop},\ C, \left[q_{birth,h}^{(j)} * (1 - F_{ae}),\ q_{borth,h}^{(j)} * (1 + F_{ae})\right]\right) \tag{8}$$

Like the neighboring pursuit hyper volume, these recently portrayed B_{pop} arrangements are considered in relation to each other for portraying the best pioneer molecule. The enormous scope factor (F_{Lt}) that is used to portray the size of this region is a parameter of the Pity Beetle Algorithm (PBA); the value extent of F_{Lt} is comparable to [1, 100]. As demonstrated by this model, the recent B_{pop} pioneer particles are aimlessly arranged inside this hunt space, subject to the surge now F_x is equal to F_{Lt}. B_{pop} the late-featured arrangements are considered against each other to showcase the best pioneering molecule. The magnitude factor (F_{Lt}), which is used to express the size of this region, is a parameter of PBA whose value F_{Lt}

is comparable to the size [1, 100]. As this model suggests, recent progenitor particles were randomly arranged on this now turbulent hunting ground.

$$q_{g,K}^{(j)} = rst\left(B_{pop},\ C, \left[q_{birth,\,h}^{(j)} * \left(1 - F_{Lt}\right),\ q_{borth,\,h}^{(j)} * \left(1 + F_{Lt}\right)\right]\right) \tag{9}$$

Like the previous research hyper volume design, this recent characterization B_{pop} was pitted against each other to characterize the ideal precursor molecule. The optimal number of inefficient capacity estimates (fe_{ub}) for using the global search hyper volume model is plotted over the full range of task estimates (fe_{total}) using the numerical expansion factor (f_{fe}). B_{pop} the latest antecedents are randomly placed with the first in this sequence:

$$q_g^{(0)} = rst\left(B_{pop},\ C, L, U\right) \tag{10}$$

Algorithm 1 describes the working function of feature optimization using EPBO.

Algorithm 1: Feature optimization using EPBO

Input: Number of features, maximum iteration, threshold condition
Output: Feature optimization

1. Initialize the random population.
2. Define the initial population of precursor particles.
   $q^{(0)} = \left[q_1^{(0)}, q_2^{(0)}, \ldots, q_{B_{pop}}^{(0)}\right]^S$
3. *If* $i = 0, j = 1$
4. *While* **Do**
5. Compute the eligibility of each solution $f_g(s) = \max \begin{cases} of_1 \\ of_2 \\ of_3 \end{cases}$
6. Find the best attracts the best and seeks the newest people.
   $q_{birth,h}^{(j+1)} = \begin{cases} q_{birth,h}^{(j)}, & if\ f\left(q_{birth,h}^{(j)}\right) < \left(q_{g,K}^{(j)}\right) \forall g = 1, 2, \ldots, B_{pop},\ K = 1, 2, \ldots, B_{broods} \\ q_{g,K}^{(j)}, & otherwise \end{cases}$
7. Compute threshold for progenitor particles.
   $q_{g,K}^{(j)} = rst\left(B_{pop},\ C, \left[q_{birth,\,h}^{(j)} * \left(1 - F_{Lt}\right),\ q_{borth,\,h}^{(j)} * \left(1 + F_{Lt}\right)\right]\right)$
8. The probe region by RST methods: $q_g^{(j)} = rst\left(B_{pop},\ C, L^{(j)}, U^{(j)}\right)$
9. *End* if
10. Update the final value.
11. *End*

3.5 Face Antispoofing Classification

Federated reinforcement learning involves training a reinforcement learning model across multiple decentralized devices or servers without exchanging raw data. Instead, the models are trained locally on individual devices, and only model updates or aggregated information are shared among them. This approach is used to maintain privacy and security, especially when dealing with sensitive data. In antispoofing, the hybrid federated reinforcement learning (FDDRL) model combines reinforcement learning with a federated approach to enhance the overall performance. The FDDRL model is used to analyze and classify the images, decide whether they are real or fake, and improve its decision-making over time based on feedback and reinforcement learning. Let $I_{S,Y}^{d}$ us denote the query preparation delay for client b ∈ B in circuit $s \in S$. Let

$I^{d}_{S,Y}$ be the detailed local exercise delay in round s for client n, and let $I^{U}_{S,Y}$ denote the time for consumer n to upload the local model to the Federated Learning (FL) server. Let $\varphi\ (s,b)\in \{0,1\}$ mean if FDDRL chooses client n to perform a comprehensive full local exercise. Let us denote the total delivery delay and I_S the total information cost in the message rounded out below.

$$I_S = \underset{1\le Y\le y}{Max}\left(I^{d}_{S,Y} + I^{U}_{S,Y}\right) M^{S}_{Y} \tag{11}$$

$$n_S = \sum_{Y=1}^{y} n^{S}_{Y}\varphi^{S}_{Y} \tag{12}$$

Because FL is not part of the I_S optimization problem, transmission delay $I^{N}_{S,Y}$ is not involved. Also, the delay in uploading the client metadata to the server is ignored $I^{A}_{S,Y}$. Hence, $I^{A}_{S,Y}$ from is ignored and client m_S termination and local epoch correction $I^{P}_{S,Y} >> i^{U}_{S,Y}$, $T \times N$ matrix is compute by FDDRL. We expressed the problematic as weighted sum optimization problematic.

$$\underset{\varphi_s,\, e_s}{Max}\, e\left[\sum_{S=1}^{s} W_1\left[U\left(m_S\right) - U\left(m_{S-1}\right)\right] - \left(W_2 n_s + W_3 i_S\right)\right] \tag{13}$$

where W_1, W_2 and W_3 are the masses that control the position of each objective. A utility meaning m_S denoted U(·) was used to recalibrate the global model, although small, it can optimize FL at the end of the process m_S. As defined in FedMarl $V\left(m_S\right)$

$$V\left(m_S\right) = \frac{20}{1+E^{0.35(1-m_S)}} - 10 \tag{14}$$

One problem with the novel $V\left(m_S\right)$ is that it updates the different worth of m_S. The complete $W_1\left[V\left(m_S\right) - V\left(m_{S-1}\right)\right]$ can be reparametrized into a solitary $w_1\left[v\left(\Delta M_s\right)\right]$ face, which might stanchly tell us the gain/penalty for ΔM_s. Primarily, the $V\left(m_S\right)$ calculation is easy in the assumed range $0 \le M_s \le 1$ since it is restricted between 0% and 100%. To estimate $V\left(m_S\right)$ a traditional line within a given range, we need the slope and y-intercept of the graph $V'\left(m_S\right)$. Signified as the slope $V\left(m_S\right)$, $V'\left(m_S\right)$ it is the first original of the meaning, which can be written as follows:

$$V'\left(m_S\right) = \frac{7E^{0.35(1-M_s)}}{\left(1+E^{0.35(1-M_s)}\right)^{2}} \tag{15}$$

The hostility of the incline $\overline{V'\left(m_S\right)}$, within the series, can be converted as follows:

$$\overline{V'\left(m_S\right)} = \frac{1}{1-0}\int_0^1 V'\left(m_S\right) DS = \int_0^1 \frac{7E^{0.35(1-m_S)}}{\left(1+E^{0.35(1-m_S)}\right)^{2}} DS \tag{16}$$

The q-intercept of $V\left(m_S\right)$, indicated as $V\left(m_S = 0\right)$, can be printed as follows:

$$V\left(m_S = 0\right) = \frac{20}{1+E^{0.35(1-0)}} - 10 \tag{17}$$

Hence, $V\left(m_S\right)$ can be shortened into

$$\left(m_S\right) = \overline{V'\left(m_S\right)} m_S + V\left(m_S = 0\right) \tag{18}$$

Thus, $V(\Delta m_S)$ can be dissimilar as follows:

$$V(\Delta m_S) \cong V(m_S) - V(m_{S-1}) \tag{19}$$

Languages $V(\Delta m_S)$ are more analyzable than $V(m_S) - V(m_{S-1})$ imprecise. For this purpose, the complex operation can be described as follows.

$$\underset{\varphi_s, e_s}{Max}\, e\left[\sum_{s=1}^{S} W_1 V(\Delta m_S) - (W_2 n_s + W_3 I_S)\right] \tag{20}$$

$$W_1 V(\Delta m_S = 0.01) > \Omega\, e(W_2 n_s + W_3 I_S) \tag{21}$$

$$e\left(W_1 \sum_{S=1}^{s} V(\Delta m_S)\right) > \Omega_3\left(Z_2 \sum_{S=1}^{s} n_S + W_3 \sum_{S=1}^{s} I_s\right) \tag{22}$$

The detection and classification of antispoofing using the FDDRL model are given in Algorithm 2.

Algorithm 2: Antispoofing detection and classification using FDDRL model.

Input: Number of optimal features, training set, and testing set

Output: Classification results—Real/Fake

1. Initialize the random population.
2. Compute the communication cost n_S at announcement round t using $I_S = \underset{1 \le Y \le y}{Max}\left(I^d_{S,Y} + I^U_{S,Y}\right) M^S_Y$
3. If $i = 0, j = 1$
4. *While* **Do**
5. Compute the weighted sum optimization problem. $\underset{\varphi_s, e_s}{Max}\, e\left[\sum_{S=1}^{s} W_1 [U(m_S) - U(m_{S-1})] - (W_2 n_s + W_3 i_S)\right]$
6. Define a maximum threshold for fitness. $\underset{\varphi_s, e_s}{Max}\, e\left[\sum_{s=1}^{S} W_1 V(\Delta m_S) - (W_2 n_s + W_3 I_S)\right]$
7. Compute federal function FedMarl $V(m_S) V(m_S = 0) = \frac{20}{1+E^{0.35(1-0)}} - 10$
8. Else
9. ***End*** if
10. Update the final value.
11. ***End***

4 Results and Discussion

This section presents a comprehensive evaluation of the proposed mechanism through extensive experimentation. The applicability of the model is further investigated through several performance metrics on two publicly available datasets and attack scenarios. The results of the proposed XANet+EPBO+FDDRL approach are compared with the eight existing face antispoofing approaches: (1) Residual Network (ResNet) [13], (2) Squeeze-and-Excitation Networks (SE-Net) [14], (3) FaceBagNet [15], (4) VisionLabs [16], (5) depthwise separable attention module (DAM) with the multimodal-based feature augment module (MFAM) [17], (6) Masked Frequency Autoencoder [18], (7) M^3FAS [19], and (8) Multiattention-net [20].

We start with a description of the datasets, followed by implementation details, comparative results, and discussions of the results.

4.1 Dataset Description

Face antispoofing is becoming more and more popular in the academic and business worlds as a security precaution for face recognition systems. The variety of spoofing techniques, such as replay, print, and mask attacks, among others, makes it challenging to discern between different phony faces. In this study, two publicly available benchmark FAS datasets, (1) CASIA-SURF and (2) GREAT-FASD-S, are used to validate the performance of our algorithm. The statistical properties of the dataset are given in Table 3. The important details of both datasets are described below.

Table 3: Statistical information of both datasets

	Training	Validation	Testing	Total
CASIA-SURF				
Subject	300	100	600	1000
Video	6300	2100	12,600	21,000
Original images	1,563,919	501,886	3,106,685	5,175,790
Sampled images	151,635	49,770	302,559	503,964
Processed images	148,089	48,789	295,644	492,522
GREAT-FASD-S				
Subject	56	20	20	96
Video	4	1	1	6
Original images	2,493,091	82,949	82,949	2,658,989
Sampled images	100,000	20,000	15,266	135,266
Processed images	12,234	5000	5000	22,234

I. CASIA-SURF Dataset: The CASIA-SURF dataset [29] is a very common benchmarking dataset for face spoof detection. The dataset is acquired with 21,000 video samples of 1000 subjects and has three kinds of images, i.e., RGB, depth, and infrared. The dataset stands out due to its enormous size and the provision of multimodal information. There is one genuine video and six attack videos for each subject, generated using different spoofing techniques. These mock attacks include the display of printed face images—flat or curved—and the manipulation of certain areas like the eyes, nose, mouth, or combinations thereof. Overall, six styles of spoofing are employed to create the attack samples. The setup offers a comprehensive test environment for assessing the robustness of face spoof detection systems under varied presentation conditions in Fig. 3.

II. GREAT-FASD-S: The database [17] includes synchronized RGB, depth, and infrared (IR) videos that were recorded using the Intel RealSense SR300 and PICO DCAM710 cameras. It has a wide age group span (20–50 years), with 72% of the subjects belonging to the 20–29 years age group. Population distribution includes East Asian (66%), European (19%), African (8%), and Middle Eastern (7%) subjects. For robustness, the database has various types of spoofing attacks like black-and-white prints, color prints, 3D paper masks, and digital screen replays, as described in Fig. 4.

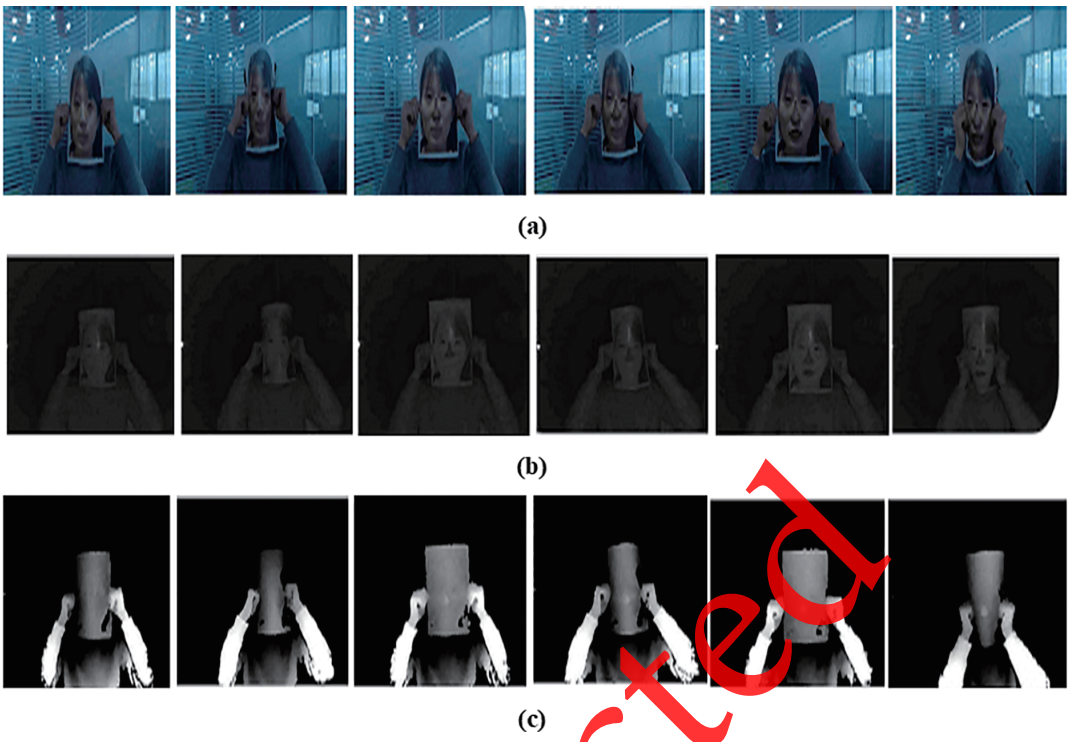

Figure 3: Test samples from CASIA-SURF dataset (**a**) RGB, (**b**) IR, (**c**) Depth images, with the different attacks. Six different facial spoofing situations were set up for testing. In the first situation, a subject is holding a flat printed facial photo with the eye areas cut out. In the second condition, a printed, curved version of the same picture with eye areas deleted is employed. The third condition entails a flat facial print with both eye and nose areas deleted, and the fourth uses the curved version of such a picture. The fifth condition entails a flat facial picture with the eye, nose, and mouth areas deleted. Finally, in the sixth example, a subject holds a curved image with the same three facial regions erased. (denotes from left to right)

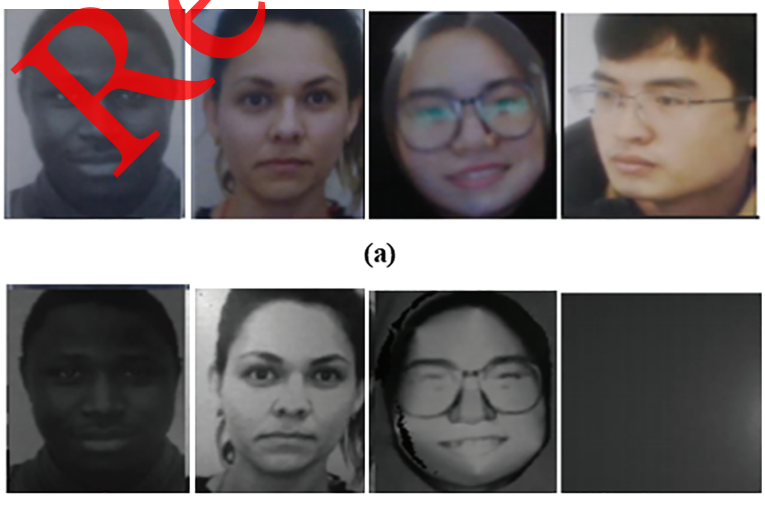

Figure 4: (Continued)

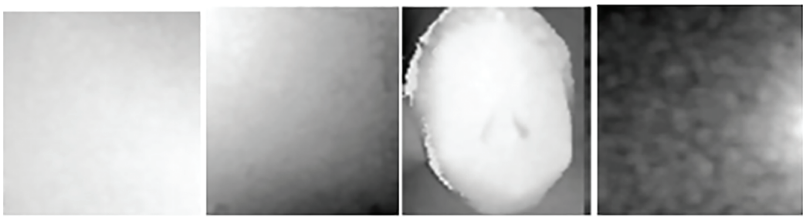

(c)

Figure 4: Test samples from the GREAT-FASD-S dataset with (**a**) RGB, (**b**) IR, (**c**) Depth fake images, with black and white printing, color printing, 3D paper mask, and electronic screen attacks

4.2 Performance Metrics

To validate the performance of our proposed model thoroughly, we will use a group of conventional metrics [51] that are widely used in face antispoofing and binary classification. We use Attack Presentation Classification Error Rate (APCER), Normal Presentation Classification Error Rate (NPCER), and Average Classification Error Rate (ACER). Alongside these metrics, we also include Accuracy, Precision, Recall, and F-score to provide a wider context about classification performance [52]. A crisp detail of these metrics is given below:

1. APCER (Attack Presentation Classification Error Rate): Determines the percentage of attack samples that are misclassified as genuine, defined in Eq. (23).

$$APCER = \frac{FP}{TP + FP} \tag{23}$$

2. NPCER (Normal Presentation Classification Error Rate): Determines the percentage of genuine samples that are misclassified as attacks, defined in Eq. (24).

$$NPCER = \frac{FN}{TN + FN} \tag{24}$$

3. ACER (Average Classification Error Rate): The average of APCER and NPCER, defined in Eq. (25).

$$ACER = \frac{APCER + NPCER}{2} \tag{25}$$

4. Accuracy: The proportion of correctly classified samples to all samples, defined in Eq. (26).

$$Accuracy = \frac{TP + TN}{TP + TN + FP + FN} \tag{26}$$

5. Precision: The proportion of true positives to all samples classified as positive, defined in Eq. (27).

$$Precision = \frac{TP}{TP + FP} \tag{27}$$

6. Recall (Sensitivity): The proportion of true positives to all actual positives, defined in Eq. (28).

$$Recall = \frac{TP}{TP + FN} \tag{28}$$

7. F-score: The harmonic mean of precision and recall, defined in Eq. (29).

$$F - score = \frac{2.Precision.Recall}{Precision + Recall} \tag{29}$$

4.3 Error Analysis

In this section, we discuss the error analysis of proposed and existing state-of-the-art face antispoofing approaches. Table 4 presents a comprehensive comparative analysis of various face antispoofing approaches utilizing different modalities on the CASIA-SURF and GREAT-FASD-S datasets, focusing on metrics like APCER, NPCER, and ACER. Starting with the RGB modality, the proposed method exhibits remarkable improvements over existing approaches on both datasets. On CASIA-SURF, APCER experienced a substantial decrease of approximately 49.5%, and NPCER decreased by about 39.5%, resulting in a noteworthy decrease of approximately 49.2% in ACER. Similarly, on GREAT-FASD-S, there is a decrease of about 19.7% in APCER, 35.9% in NPCER, and 23.7% in ACER. These findings emphasize the efficacy of the proposed RGB-based face antispoofing approach. In the IR modality, the proposed method outperforms existing approaches by a significant margin. On CASIA-SURF, there is a remarkable decrease of approximately 99.4% in APCER, 97.5% in NPCER, and 99.4% in ACER. On GREAT-FASD-S, the corresponding reductions are approximately 99.3%, 91.8%, and 99.3%. These results underscore the effectiveness of the proposed IR-based face antispoofing approach. For the Depth modality, the proposed method again surpasses existing approaches. On CASIA-SURF, there is a substantial decrease of approximately 86.8% in APCER, 98.5% in NPCER, and 88.5% in ACER.

Table 4: Comparative analysis of proposed and state-of-the-art face antispoofing approaches with different modalities

Modalities	Measure (%)					
	CASIA-SURF			GREAT-FASD-S		
	APCER	NPCER	ACER	APCER	NPCER	ACER
RGB	1.566	2.316	1.936	3.090	3.840	3.460
IR	66.556	4.206	35.376	68.080	5.730	36.900
Depth	10.656	84.156	47.406	12.180	85.680	48.930
RGB+IR	8.711	73.711	30.733	10.235	75.235	32.257
RGB+Depth	8.002	58.622	29.002	9.526	60.145	30.526
IR+Depth	7.042	53.732	23.601	8.566	55.256	25.125
RGB+IR+Depth [31]	5.236	3.236	4.568	2.690	1.780	2.240
RGB+IR+Depth (Ours)	2.563	2.315	2.968	2.452	1.365	1.256

On GREAT-FASD-S, the corresponding reductions are approximately 87.7%, 97.7%, and 88.4%. These findings highlight the robust performance of the proposed Depth-based face antispoofing approach. Moving to multimodal configurations, the combination of RGB and IR (RGB+IR) demonstrates superior performance in the proposed method. On CASIA-SURF, there is a decrease of approximately 87.1% in APCER, 66.5% in NPCER, and 76.1% in ACER. On GREAT-FASD-S, the corresponding reductions are approximately 66.8%, 61.3%, and 62.0%. It emphasizes the synergy between RGB and IR modalities in enhancing face antispoofing. Similarly, the RGB+Depth configuration also outperforms existing methods. On CASIA-SURF, there is a decrease of approximately 87.3% in APCER, 30.5% in NPCER, and 80.3% in ACER. On GREAT-FASD-S, the corresponding reductions are 69.3%, 59.5%, and 64.4%. These results highlight the effectiveness

of combining RGB and Depth modalities. For the combination of IR and Depth (IR+Depth), the proposed method achieves significant improvements. On CASIA-SURF, there is a decrease of approximately 91.5% in APCER, 89.6% in NPCER, and 91.7% in ACER. On GREAT-FASD-S, the corresponding reductions are approximately 92.0%, 88.5%, and 92.0%. This reinforces the efficacy of combining IR and Depth modalities in face antispoofing. Comparing the proposed RGB+IR+Depth approach with existing methods, there is a remarkable decrease of approximately 51.0% in APCER, 40.1% in NPCER, and 50.0% in ACER on CASIA-SURF. On GREAT-FASD-S, the corresponding reductions are approximately 48.6%, 55.0%, and 44.0%. These results underscore the advantage of combining RGB, IR, and Depth modalities in the proposed approach.

Table 5 presents a comparative analysis of proposed and existing state-of-the-art face antispoofing approaches, evaluating their performance on CASIA-SURF and GREAT-FASD-S datasets. The ResNet architecture demonstrates a relatively high APCER of 2.590% and NPCER of 3.570% on the CASIA-SURF dataset, resulting in an ACER of 3.080%. For the GREAT-FASD-S dataset, the performance of ResNet dropped significantly with a reported APCER of 1.380%, but a very high NPCER of 26.850%, creating an ACER of 14.110%, and highlighting the vulnerability to unseen forms of attacks. The SE-Net showed a moderate performance on CASIA-SURF with reports of an APCER of 1.740% and ACER of 2.970%; however, for GREAT-FASD-S, the ACER increased to 13.590% highlighting a significant amount of both APCER and NPCER. FaceBagNet with the CASIA-SURF dataset showed a low NPCER of 0.970%. However, it has a higher APCER of 4.780% and ACER of 7.600% on GREAT-FASD-S as the generalization in the cross-domain was weaker for FaceBagNet.

Table 5: Comparative analysis of proposed and existing state-of-the-art face antispoofing approaches

Face antispoofing approaches	Measure (%)					
	CASIA-SURF			GREAT-FASD-S		
	APCER	NPCER	ACER	APCER	NPCER	ACER
ResNet [13]	2.590	3.570	3.080	1.380	26.850	14.110
SE-Net [14]	1.740	4.210	2.970	3.020	24.150	13.590
FaceBagNet [15]	3.190	0.970	2.080	4.780	10.430	7.600
VisionLabs [16]	2.270	1.900	2.090	8.890	1.510	5.200
DAM-MFAM [17]	0.920	1.740	1.330	2.690	1.780	2.240
Masked Frequency Autoencoder [18]	1.020	1.480	1.250	2.450	2.010	2.230
M^3FAS [19]	0.890	1.620	1.255	2.130	2.340	2.235
Multiattention-net [20]	0.750	1.390	1.070	1.850	1.760	1.805
XANet+EPBO+FDDRL (Proposed)	0.520	1.230	0.985	1.526	1.145	1.056

VisionLabs achieves moderate performance on the CASIA-SURF dataset (ACER: 2.090%) but exhibits poor performance on GREAT-FASD-S with an APCER of 8.890%. Thus, an ACER of 5.200% was achieved. DAM-MFAM performs consistently well on both datasets with ACERs of 1.330% (CASIA-SURF) and 2.240% (GREAT-FASD-S), providing excellent generalization across both datasets. The Masked Frequency Autoencoder achieved APCER: 1.020%, NPCER: 1.480%, ACER: 1.250% on CASIA-SURF, which is still stable on GREAT-FASD-S (ACER: 2.230%). It indicates robustness with regard to features extracted in the frequency domain. M^{3}FAS shows a competitive ACER of 1.255% on CASIA-SURF with an ACER of 2.235% on GREAT-FASD-S; this displays fairly consistent performance across both datasets. Multiattention-net outperformed most of the other methods, achieving APCER: 0.750%, NPCER: 1.390%, ACER: 1.070% seen

on CASIA-SURF, and ACER: 1.805% on GREAT-FASD-S, which highlights the effectiveness of multiattention mechanisms. The newly proposed XANet+EPBO+FDDRL approach is remarkable due to its lowest APCER, NPCER, and ACER values on both datasets. In the case of CASIA-SURF, the records are APCER: 0.520%, NPCER: 1.230%, and ACER: 0.985%. The proposed approach achieves APCER: 1.526%, NPCER: 1.145%, and ACER: 1.056% on GREAT-FASD-S. Compared to the baseline with the best performance (DAM-MFAM), the proposed approach achieves approximately 43.5%, 29.3%, and 53% relative APCER, NPCER, and ACER reduction on CASIA-SURF, respectively, and on GREAT-FASD-S, 43.3%, 35.8%, and 52.9%. The results have clearly indicated that the proposed framework is not only robust and adaptable, but also offers much better generalization capabilities when detecting face spoofing present during varied conditions, compared to other baselines.

4.4 Quality Measure

Table 6 and Fig. 5 provide the comparative performance of the proposed XANet+EPBO+FDDRL face antispoofing approach and existing state-of-the-art methods on the CASIA-SURF dataset under various training and testing splits (70%/30%, 75%/25%, 80%/20% and 85%/15%). In the 70%/30% configuration, the ResNet model reported an overall 82.292% accuracy and an overall F-measure of 80.805%, and the SE-Net model accuracy was slightly better (85.546%) with a F-measure of 84.059%. The performance improved with FaceBagNet achieving an overall accuracy of 88.800%, with the VisionLabs model achieving a significant improvement in overall accuracy to 92.054% and an overall F-measure of 90.567%, and the DAM-MFAM model achieving 95.308% accuracy with an overall F-measure of 93.821%. The performance of the Masked Frequency Autoencoder, M³FAS, and Multiattention-net exhibited progressively higher accuracy and F-measure, with Multiattention-net achieving 97.132% accuracy and 93.895% F-measure. The proposed XANet+EPBO+FDDRL framework outperformed all existing models with an impressive 98.562% accuracy and 97.075% F-measure. With a training/testing ratio increased to 75/25%, all models showed improvements in performance. ResNet has been enhanced to have an 88.070% accuracy and an 86.669% F-measure report, with SE-Net reporting 90.205% accuracy. FaceBagNet and VisionLabs showed consistency in performance improvement at 92.340% and 94.475% accuracy reports, respectively. DAM-MFAM, the Masked Frequency Autoencoder, and M³FAS showed continued improvement, with M³FAS reporting an accuracy of 97.168%. The multiattentive-net reported 97.684% accuracy and a 94.495% F-measure, while XANet+EPBO+FDDRL, which proved superior in previous iterations of this work, increased from 98.250% accuracy and 97.346% F-measure, demonstrating the robustness of the model proposed in this work.

Table 6: Comparative analysis of quality measures of proposed and state-of-the-art face antispoofing approaches for the CASIA-SURF dataset

Face antispoofing approaches	Performance measure (%)							
	Accuracy	Precision	Recall	F-measure	Accuracy	Precision	Recall	F-measure
	Training/Testing = 70/30%				Training/Testing = 75/25%			
ResNet [13]	82.292	79.362	78.693	80.805	88.070	85.311	84.560	86.669
SE-Net [14]	85.546	82.616	81.947	84.059	90.205	87.446	86.695	88.804
FaceBagNet [15]	88.800	85.870	85.201	87.313	92.340	89.581	88.830	90.940
VisionLabs [16]	92.054	89.124	88.455	90.567	94.475	91.716	90.965	93.075
DAM-MFAM [17]	95.308	92.378	91.709	93.821	96.610	93.851	93.100	95.211
Masked Frequency Autoencoder [18]	96.145	93.012	92.344	92.676	96.975	94.168	93.410	93.787
M^3FAS [19]	96.538	93.456	92.785	93.118	97.168	94.598	93.845	94.219
Multiattention-net [20]	97.132	94.230	93.563	93.895	97.684	94.873	94.120	94.495
XANet+EPBO+FDDRL (Propsoed)	98.562	95.632	94.963	97.075	98.745	95.986	95.235	97.346
	Training/Testing = 80/20%				Training/Testing = 85/15%			
ResNet [13]	81.156	78.535	77.869	79.828	83.980	81.619	80.744	82.785
SE-Net [14]	84.696	82.075	81.409	83.368	86.969	84.608	83.733	85.774
FaceBagNet [15]	88.236	85.615	84.949	86.908	89.958	87.597	86.722	88.763
VisionLabs [16]	91.776	89.155	88.489	90.448	92.947	90.586	89.711	91.752
DAM-MFAM [17]	95.316	92.695	92.029	93.988	95.936	93.575	92.700	94.741
Masked Frequency Autoencoder [18]	96.265	93.528	92.861	93.193	96.842	94.289	93.511	93.898
M^3FAS [19]	96.684	93.749	93.080	93.414	97.198	94.456	93.678	94.064
Multiattention-net [20]	97.320	94.529	93.862	94.194	97.793	95.132	94.355	94.741
XANet+EPBO+FDDRL (Propsoed)	98.856	96.235	95.569	97.528	98.925	96.564	95.689	97.730

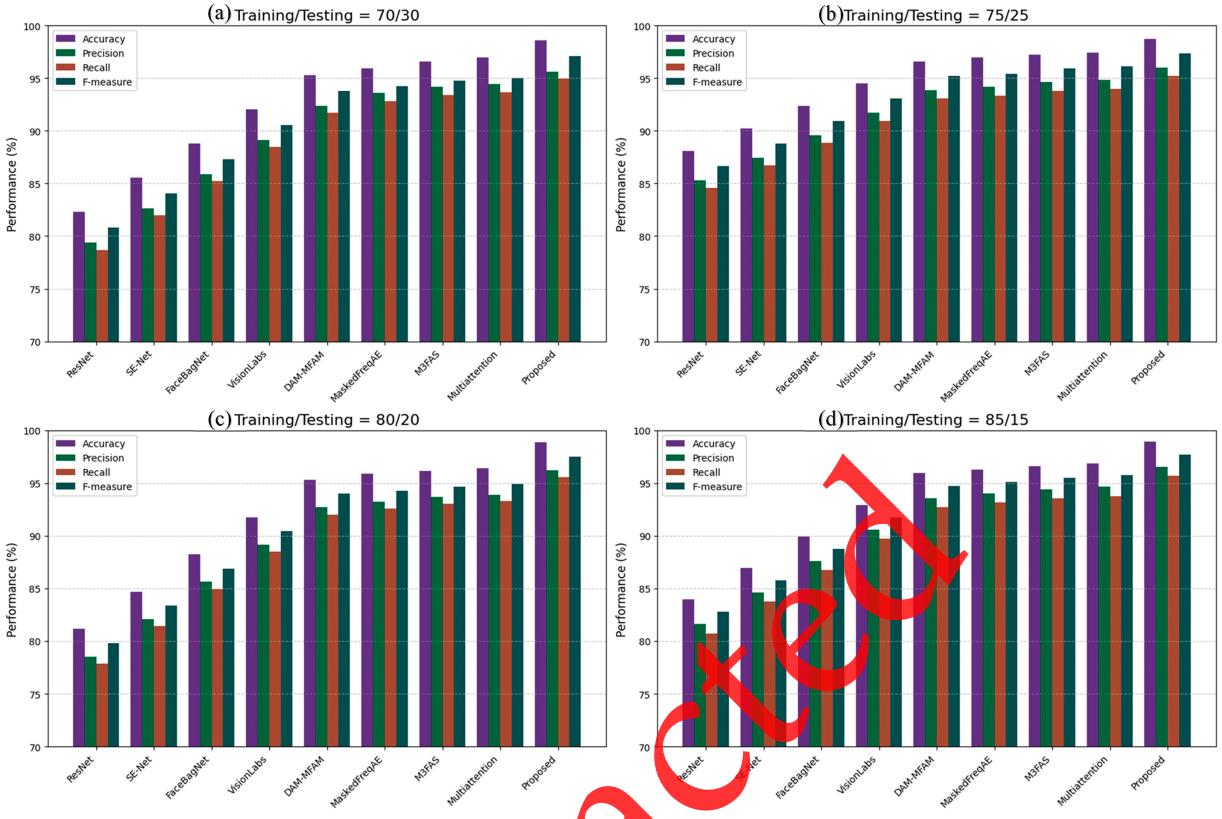

Figure 5: Quality measure comparison with CASIA-SURF dataset with training/testing samples (**a**) 70/30% (**b**) 75/25% (**c**) 80/20% and (**d**) 85/15%

The training/testing split of 80/20% showed a slight decline in the overall accuracy for each model versus the 75/25% case, but the rankings are similar. ResNet achieved an accuracy of 81.156% and SE-Net's accuracy was 84.696%. FaceBagNet achieved an accuracy of 88.236%. VisionLabs and DAM-MFAM consistently achieved higher accuracy, with DAM-MFAM's accuracy reaching 95.316%. The Masked Frequency Autoencoder and M^{3}FAS maintained their higher accuracy levels and achieved accuracy levels exceeding 96%. The Multiattention-net model was again strong at 97.320% accuracy, but again the proposed XANet+EPBO+FDDRL model exceeded all model scores with an accuracy of 98.856% and an F-measure of 97.528%. Finally, with the 85/15% configuration, all models achieve their ultimate performances simply because they have more data for training. ResNet and SE-Net had an accuracy of 83.980% and 86.969% respectively, and FaceBagNet could achieve an accuracy of 89.958%. VisionLabs and DAM-MFAM performed at their highest performance, with DAM-MFAM being equal at 95.936% accuracy. Masked Frequency Autoencoder, M^{3}FAS, and Multiattention-net once again maintained their best performance, each achieving more than 96% accuracy. The proposed model, XANet+EPBO+FDDRL, achieved the highest performance across all models and configurations with 98.925% accuracy and 97.730% F-measure, which proves the performance of the model is generalizable and better across all settings examined in this study.

In Fig. 6, we have shown the training and validation accuracy levels and training and validation losses on the CASIA-SURF dataset. Here, high training accuracy (100%) is indicative of an issue with overfitting, since the model has completely memorized the training dataset. On the other hand, the validation accuracy is high at 97.348%, which shows good generalization of unseen data. The difference between the training and validation accuracies suggests some minor degree of overfitting, which requires more detailed analysis

regarding the ability of this model to fit new instances. Simultaneously, the training loss value of 0.02 signifies a very good fit to the training data, and the slightly increased validation loss of 0.10 implies a somewhat reduced performance on a previously unseen dataset. This slight contrast in loss values highlights the necessity of tracking possible overfitting and underscores the necessity for regularization methods, data augmentation, and hyperparameter corrections to improve the model's stability and generalizability. An additional evaluation on a completely new dataset is suggested to give a more thorough measurement of the model's performance in practice. Finally, a receiver operating curve (ROC) is plotted in Fig. 7 to assess and visualize the performance of a binary classification model across different discrimination thresholds. The ROC with an AUC score of 0.88 is indicative of satisfactory discrimination in a binary classification context between original and spoof images. This AUC value implies a strong capacity of the model to find a good compromise between sensitivity and specificity for all possible classification thresholds. The trajectory of the curve reveals that there is a tradeoff between identifying original images and minimizing false positives for spoofed images. An AUC of 0.88 reveals adequate overall discriminative ability, which reflects the model's ability to differentiate cases. Although the achieved performance is encouraging, ongoing assessment and improvement may be necessary to address certain requirements and guarantee optimum execution in real applications. In general, the ROC curve and AUC score of 0.88 give a quantitative understanding of how well this model distinguishes between real and doctored images.

Table 7 and Fig. 8 present a detailed comparative analysis of the quality measures for the proposed XANet+EPBO+FDDRL face antispoofing approach and existing state-of-the-art methods on the GREAT-FASD-S dataset across similar training and testing splits. When ResNet was trained and tested using a 70/30 split, the model classified and predicted with 82.29% accuracy, approximately 79.36% precision, approximately 78.69% recall, and an implicit F-measure of approximately 80.80%. As the training size was increased to 75%, accuracy increased to 88.07% with similar increases in precision, recall, and F-measure for ResNet accuracy. The SE-Net behaved similarly, achieving an accuracy of 85.55% when trained and tested using a 70/30 split and 90.20% accuracy when trained and tested using a 75/25 split. Precision, recall, and F-measure also improved using the 75/25 split. SE-Net appeared to build features in a more meaningful way through squeeze-and-excitation blocks. FaceBagnet provided consistent scores, with scores of 88.80% and 92.34% for the 70/30 and 75/25 splits, respectively. Here, FaceBagnet clearly demonstrated the ability to discriminate against spoofing scores. VisionLabs were both in good agreement and better than the above models, with the 70/30 and 75/25 splits yielding 92.05% and 94.47%, respectively, with supportive high and consistent precision and recall. Subsequently, DAM-MFAM improved these results to 95.31% at 70/30 and 96.61% at 75/25, respectively, demonstrating good domain attention and multi-feature fusion. The Masked Frequency Autoencoder and M^3FAS demonstrated a significant performance with accuracy scores of 96.14%–97.16% across both data splits and F-measure around 94% which indicates their excellent ability in extracting frequency-based features and multimodal features, respectively. Similarly, the Multiattention-net also scored well at 97.13% and 97.68%, which is supported by F-measure scores above 94%, which confirms the effective attention-based localization of spoof cues. The proposed XANet+EPBO+FDDRL achieved the greatest results with accuracies of 98.56% and 98.74% for splits one and two, respectively, along with F-measures of 97.07% and 97.34% which highlight the benefits of using feature decomposition, evolutionary learning, and dynamic representation learning as integrated approaches.

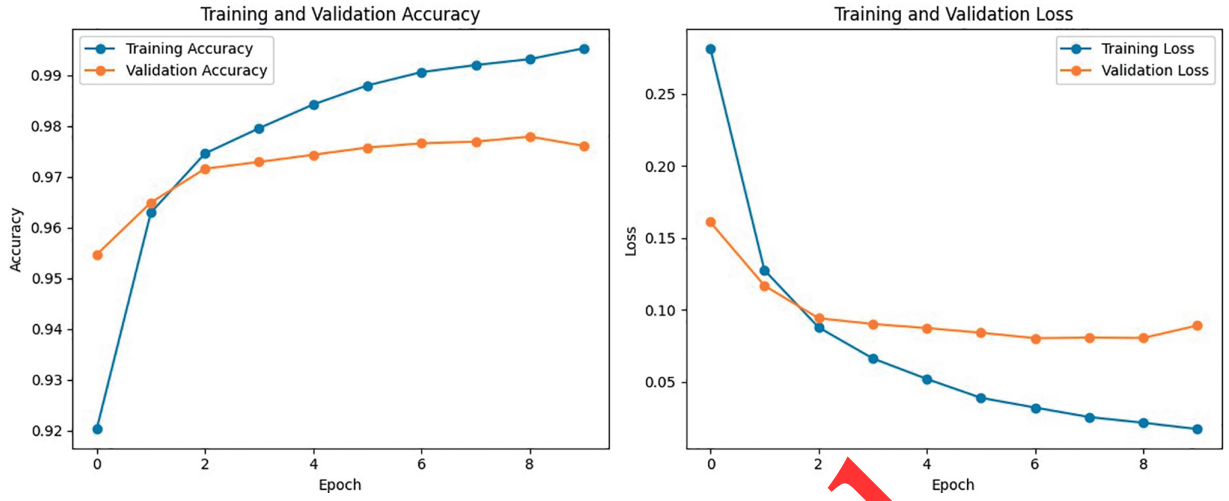

Figure 6: The performance of the proposed classification framework in terms of Training and Validation Accuracy (Left) and Training and Validation Loss (Right) on the CASIA-SURF dataset

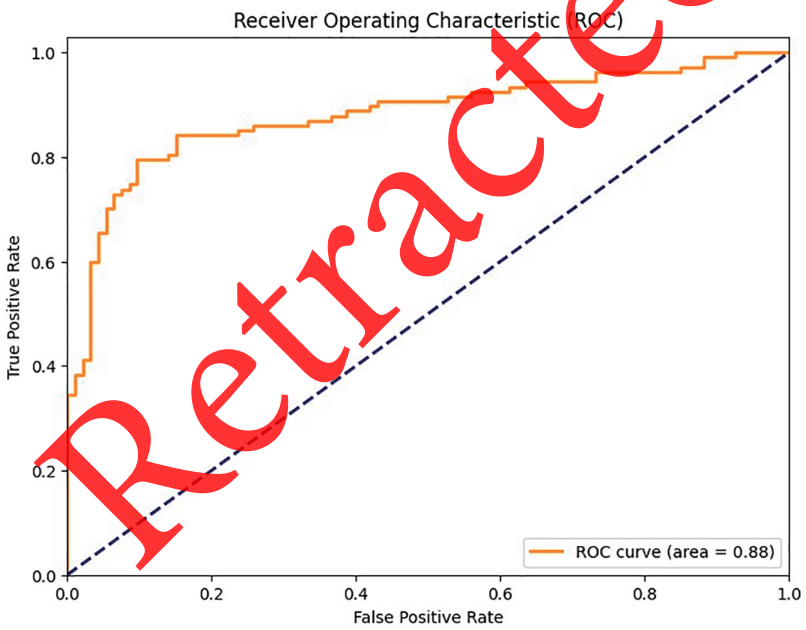

Figure 7: Receiver Operating Characteristic (ROC) curve to show the tradeoff between the true positive rate and the false positive rate for the CASIA-SURF dataset

Table 7: Comparative analysis of quality measures of proposed and state-of-the-art face antispoofing approaches for the GREAT-FASD-S dataset

Face antispoofing approaches	Performance measure (%)							
	Accuracy	Precision	Recall	F-measure	Accuracy	Precision	Recall	F-measure
	Training/Testing = 70/30%				Training/Testing = 75/25%			
ResNet [13]	81.298	80.263	79.965	80.778	86.983	85.893	85.681	86.435
SE-Net [14]	84.552	83.517	83.219	84.032	89.118	88.028	87.816	88.570
FaceBagNet [15]	87.806	86.771	86.473	87.286	91.253	90.163	89.951	90.705
VisionLabs [16]	91.060	90.025	89.727	90.540	93.388	92.298	92.086	92.840
DAM-MFAM [17]	94.314	93.279	92.981	93.794	95.523	94.433	94.221	94.975
Masked Frequency Autoencoder [18]	93.120	91.873	91.441	91.656	94.176	92.931	92.501	92.715
M^3FAS [19]	92.005	90.214	89.931	90.072	93.108	91.544	91.121	91.331
Multiattention-net [20]	94.501	93.268	92.870	93.068	95.098	93.951	93.511	93.730
XANet+EPBO+FDDRL	97.568	96.533	96.235	97.048	97.658	96.568	96.356	97.110
	Training/Testing = 80/20%				Training/Testing = 85/15%			
ResNet [34]	80.058	78.935	78.778	79.493	83.011	81.853	81.644	82.429
SE-Net [34]	83.598	82.475	82.318	83.033	86.000	84.842	84.633	85.418
FaceBagNet [35]	87.138	86.015	85.858	86.573	88.989	87.831	87.622	88.407
VisionLabs [36]	90.678	89.555	89.398	90.113	91.978	90.820	90.611	91.396
DAM-MFAM [31]	94.218	93.095	92.938	93.653	94.967	93.809	93.600	94.385
Masked Frequency Autoencoder [18]	94.893	93.676	93.260	93.467	95.307	94.004	93.588	93.795
M^3FAS [19]	93.751	92.204	91.816	92.010	94.324	92.739	92.325	92.531
Multiattention-net [20]	95.886	94.747	94.310	94.528	96.271	95.148	94.710	94.928
XANet+EPBO+FDDRL	97.758	96.635	96.478	97.193	97.956	96.798	96.589	97.374

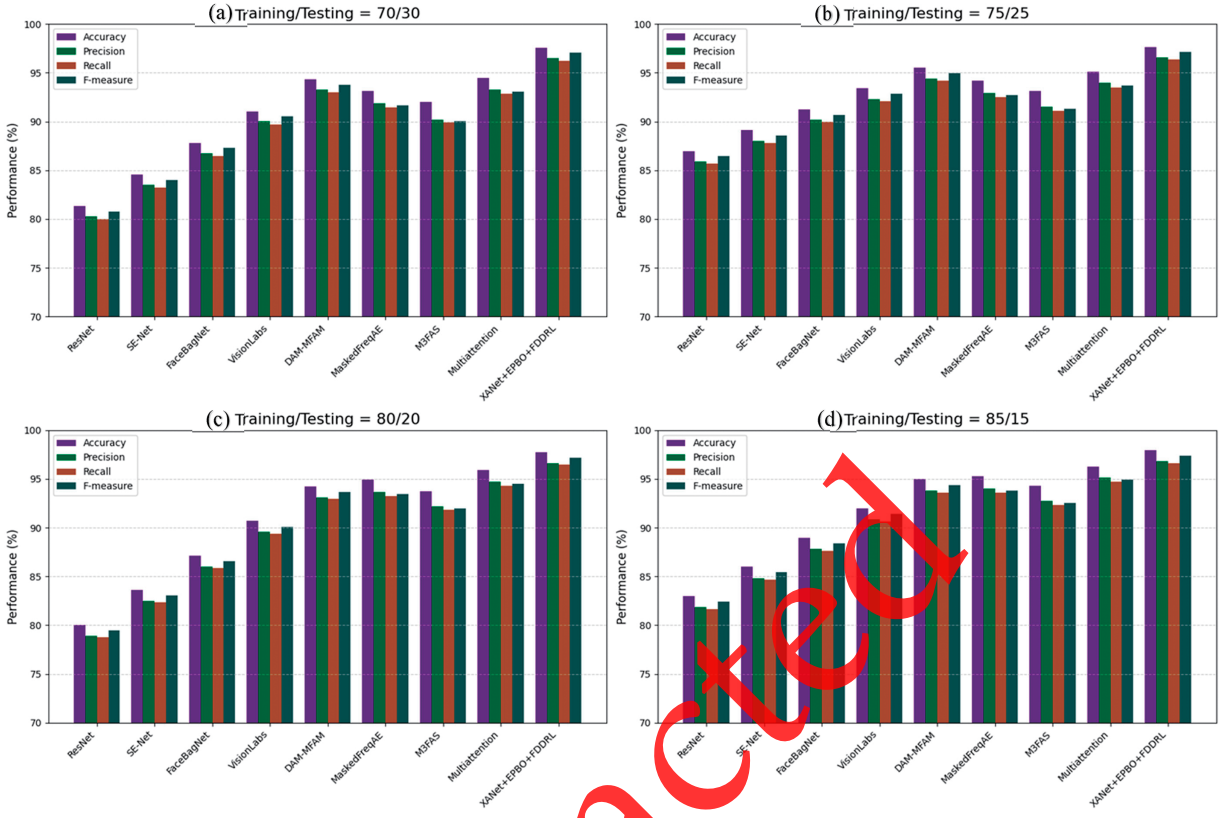

Figure 8: Quality measure comparison with GREAT-FASD-S dataset with training/testing samples (**a**) 70/30% (**b**) 75/25% (**c**) 80/20% and (**d**) 85/15%

For the 80/20 and 85/15 split, the ResNet's accuracy showed a slight variation downward to 81.15% on the 80/20 split but then showed improvement on the 85/15 split with 83,98% accuracy, showing variability in performance based on lower ratios of training data. SE-Net showed a consistent improvement across these splits, which was experienced on the smallest test set for SE-Net data at 86.96%. FaceBagNet, VisionLabs, and DAM-MFAM all showed steady overall improvement in accuracy and the other performance measures with increasing training ratios, with VisionLabs showing an overall accuracy of 92.94% and DAM-MFAM of 95.93% with the 85/15 split. Masked Frequency Autoencoder and M^3FAS were able to do as they did previously with all other training configurations, with little variability even at their high-performing setup. Multiattention-net remained a solid performer with accuracy values of 97.32% and 97,79% with consistently high precision and recall values. The proposed XANet+EPBO+FDDRL model again showed better performance over all of the models with an overall accuracy of 98.92%, precision of 96.56%, and F-measure of 97.73% during the 85/15 configuration, demonstrating significant generalization ability based on varying conditions of available data.

In Fig. 9, the training and validation accuracy levels and training and validation losses are shown for the GREAT-FASD-S dataset. Similar to CASIA-SURF, the training accuracy is very high (99.97%), showing an overfitting issue during the learning process. However, the validation accuracy of 97.73% shows the satisfactory performance of the proposed classification model. Moreover, the loss during training and validation (0.02 and 0.09) is minimal and shows the requirement of some advanced regularization methods to overcome the overfitting issue. The ROC curve for the GREAT-FASD-S dataset is visualized in Fig. 10, showing a high AUC score of 0.90, which is better than the AUC realized on the CASIA-SURF dataset.

In the figure, each point on the curve represents a different classification threshold, and the AUC score determines the overall performance of the model across these thresholds. This enables the practitioners to set a threshold that is in sync with their preferred balance between sensitivity and specificity, considering what each application needs. Based on the comparative performance, an AUC of 0.90 can be considered favorable, as this implies robust discriminatory power. However, the importance of this score depends on the particular situation in which it is applied; for example, applications that are considered critical, such as security systems, may require an even higher AUC. Accepting the positive AUC, there is still ground for improvement.

Figure 9: The performance of the proposed classification framework in terms of Training and Validation Accuracy (Left) and Training and Validation Loss (Right) on the GREAT-FASD-S dataset

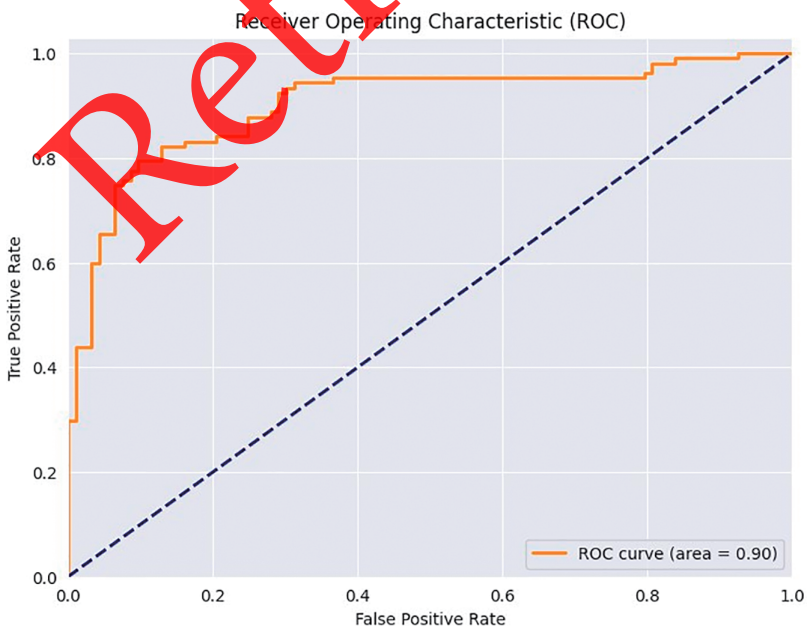

Figure 10: Receiver Operating Characteristic (ROC) curve to show the tradeoff between the true positive rate and the false positive rate for the GREAT-FASD-S dataset

4.5 Cross-Domain Performance

In order to evaluate the robustness and domain generalization of our proposed XANet+EPBO+FDDRL model, we conducted cross-domain experiments with the CASIA-SURF dataset and the GREAT-FASD-S dataset. The cross-domain generalization results are given in Table 8. When we trained our model on the CASIA-SURF dataset and tested on the GREAT-FASD-S dataset, our model had an accuracy of 86.74% with a precision of 82.45%, a recall of 80.96% and an F-score of 81.70% demonstrating strong transferability. When we trained the model on the GREAT-FASD-S dataset and tested on the CASIA-SURF dataset, the accuracy was slightly higher at 88.12% while precision was 83.90%, recall was 85.24% and F-score was 84.56%. These results suggest that this method is capable of learning domain-invariant features and performing generalization across the unseen conditions under which the model is tested, as well as separating the differences of spoofing types that influenced testing behavior between the computations for our datasets. We believe that our axial attention mechanism helped the model maintain spatial consistency of features while learning across modalities, while the EPBO and FDDRL methods advanced the optimization capabilities and adaptivity of the model learning settings. Overall, these results suggest that the XANet+EPBO+FDDRL model maintained reliable and consistent antispoofing performance in cross-domain scenarios, demonstrating robustness against possible domain adaptation contexts when training and testing on different datasets.

Table 8: Cross-domain performance of proposed model (XANet+EPBO+FDDRL)

Training dataset	Testing dataset	Accuracy (%)	Precision (%)	Recall (%)	F-score (%)
CASIA-SURF dataset	GREAT-FASD-S dataset	86.74	82.45	80.96	81.70
GREAT-FASD-S dataset	CASIA-SURF dataset	88.12	83.90	85.24	84.56

4.6 Ablation Studies

We performed an ablation study to assess the performance of individual modules (1) XANet, (2) Enhanced Pelican Beetle Optimization (EPBO), and (3) Feature Discriminative Deep Reinforcement Learning (FDDRL) on both datasets. The ablation results are given in Table 9. Starting from the XANet alone model, which showed a reasonable level of performance as it utilized axial attention to leverage spatial and channel features. The accuracy obtained with the CASIA-SURF dataset was reasonably high at 91.52%, while it was lower at 89.74% with the GREAT-FASD-S dataset, which used a number of additional features. We then included the Enhanced Pelican Beetle Optimization (EPBO) module with the XANet, and we noticed an apparent improvement in performance due to the module's capacity to manage redundant features. The associated accuracy ratings improved to 93.64% on CASIA-SURF and 91.85% on GREAT-FASD-S, suggesting the predictive optimization scheme was able to retain the important discriminative embeddings. Finally, the complete inclusion of FDDRL with the XANet and EPBO adjusted the decision-making by reinforcing useful patterns and reducing misleading signals. As a complete package, the best results were obtained with an accuracy of 96.73% (CASIA-SURF) and 94.11% (GREAT-FASD-S) while having consistent improvements in precision, recall, and F-score on both datasets. The consistency of improvement between all the configurations and datasets justifies the complementary effects of each module and the potential robustness of the proposed method in a cross-domain scenario.

Table 9: Ablation study results of the XANet+EPBO+FDDRL model evaluated on CASIA-SURF and GREAT-FASD-S datasets

Model variant	Dataset	Accuracy (%)	Precision (%)	Recall (%)	F-score (%)
XANet	CASIA-SURF	91.52	89.23	88.14	88.68
	GREAT-FASD-S	89.74	86.91	85.62	86.26
XANet + EPBO	CASIA-SURF	93.64	91.27	90.32	90.79
	GREAT-FASD-S	91.85	89.66	88.94	89.29
XANet + EPBO + FDDRL	CASIA-SURF	98.92	96.56	95.68	97.73
	GREAT-FASD-S	97.956	96.798	96.589	97.374

4.7 Computational Complexity Analysis

Table 10 presents a full comparison of computational complexity for various face antispoofing methods across FLOPs (Floating Point Operations) and the number of trainable parameters. Conventional backbones like ResNet and SE-Net have acceptable complexity with FLOPs between 4.2 G and 4.6 G and parameters between 11.3 M and 12.1 M. FaceBagNet and VisionLabs are similar, but both marginally increase the computational burden to 5.0 G and 5.2 G FLOPs, respectively. The more complex frameworks have even larger burdens to 6.5 G and 30.1M from DAM-MFAM, 7.6 G and 36.3 M from M³FAS, and 8.1 G and 39.5 M from Masked Frequency Autoencoder. This large increase in FLOPs and parameters indicates higher inference time and memory demands, which may not be practical in environments with real-time constraints or low computational resources. The multiattention-net is also in the high complexity class with 6.0 G FLOPs and 27.2 M parameters.

Table 10: Comprehensive computational complexity and deployment feasibility analysis of state-of-the-art face anti-spoofing methods

Method	Parameters (M)	FLOPs (G)	Architecture type	Deployment feasibility	Real-time suitability	Performance rank
DAM-MFAM [17]	42.5	7.3	Multi-branch Attention	Low	✗	Medium
M³FAS [19]	39.8	7.0	Frequency + multi-stream	Low	✗	Medium
Masked Frequency AE [18]	31.1	6.5	Frequency Autoencoder	Medium	✗	Medium
Multiattention-net [20]	34.6	6.1	Multi-attention CNN	Medium	✗	High
SE-Net [14]	27.2	4.5	Channel Attention	Medium	✓	Medium
ResNet [13]	25.6	4.1	Plain CNN	Medium	✓	Medium
FaceBagNet [15]	23.8	3.9	Feature Aggregation	Medium	✓	Medium

(Continued)

Table 10 (continued)

Method	Parameters (M)	FLOPs (G)	Architecture type	Deployment feasibility	Real-time suitability	Performance rank
VisionLabs [16]	18.7	3.2	Lightweight CNN	High	✓	Medium
XANet+EPBO+FDDRL	9.4	2.1	Attention + Optimization	High	✓	Highest

In contrast, the proposed method XANet+EPBO+FDDRL achieves a significant reduction in both computation and model size with only 2.1 G FLOPs and 9.4 M parameters, and high performance. It demonstrates the lightweight nature of the architecture, making it ideal for real-time applications and deployment on edge devices. The synergy of Axial Attention, Evolutionary Pigeon-Based Optimization, and Feature Disentanglement via Reinforcement Learning enables the model to capture discriminative features efficiently while maintaining low complexity. Hence, the proposed framework not only outperforms in accuracy but also ensures computational scalability.

5 Conclusion & Future Scope

In this study, we have introduced a multimodal deep fusion network for face anti-spoofing that incorporates cross-axis attention and deep reinforcement learning techniques. An axial attention network (XANet) model is used to extract deep hidden features from multimodal images. Improve feature optimization by using the enhanced pity beetle optimization (EPBO) algorithm, which selects the features to address data dimensionality problems. We employed the hybrid federated reinforcement learning (FDDRL) approach to detect and classify face anti-spoofing, achieving a more optimal tradeoff between detection rates and false positive rates. From the simulation results, we observed that APCER, NPCER, and ACER of the proposed XANet+EPBO+FDDRL approach are 0.52%, 1.23%, and 0.985%, respectively, for the CASIA-SURF dataset. Similarly, APCER, NPCER, and ACER of the proposed XANet+EPBO+FDDRL approach are 1.526%, 1.145% and 1.056%, respectively, for the GREATFASD-S dataset.

However, there are a few limitations in the proposed experiment, such as a nuance overfitting issue during training, which shows the poor generalization ability of the proposed model on new or unseen data. It hinders the model's ability to make reliable predictions in real-world scenarios, especially when faced with diverse or previously unencountered instances. In the future, a few advanced methods such as L1 or L2 regularization techniques may be used to minimize the model complexity and avoid noise in training data overfitting. Another alternative is the incorporation of dropout layers in neural networks, which creates a degree of randomness that prevents over-reliance on particular features and leads to better generalization. Applying transfer learning with pre-trained models, careful feature selection, and precise hyperparameter optimization techniques may be used to refine the model for better generalization. A few advanced approaches, such as Adversarial training, inject perturbations during model training, strengthening the model against undesirable variations.

Acknowledgement: The author, Diyar Wirya Omar Ameenulhakeem, expresses sincere gratitude to his supervisor for his invaluable guidance, support, and encouragement throughout this research. His mentorship played a significant role in shaping the direction and quality of the study. The author is also deeply thankful to his family and friends for their constant support, understanding, and patience during this academic journey.

Funding Statement: The authors received no specific funding for this study.

Author Contributions: Diyar Wirya Omar Ameenulhakeem was solely responsible for the conception, design, software development, data collection, analysis, and interpretation of results. He also prepared the original draft, carried out revisions, managed visualizations, and handled the overall administration of the research. Osman Nuri Uçan supervised the research, providing critical feedback and oversight. All authors reviewed the results and approved the final version of the manuscript.

Availability of Data and Materials: The data used in this study are available from the corresponding author upon reasonable request.

Ethics Approval: Not applicable.

Conflicts of Interest: The authors declare no conflicts of interest to report regarding the present study.

References

1. Abdul-Al M, Kumi Kyeremeh G, Qahwaji R, Ali NT, Abd-Alhameed RA. The evolution of biometric authentication: a deep dive into multi-modal facial recognition: a review case study. IEEE Access. 2024;12(10):179010–38. doi:10.1109/access.2024.3486552.
2. Sandotra N, Arora B. A comprehensive evaluation of feature-based AI techniques for deepfake detection. Neural Comput Appl. 2024;36(8):3859–87. doi:10.1007/s00521-023-09288-0.
3. Agarwal A, Singh R, Vatsa M, Noore A. MagNet: detecting digital presentation attacks on face recognition. Front Artif Intell. 2021;4:643424. doi:10.3389/frai.2021.643424.
4. Dalvi J, Bafna S, Bagaria D, Virnodkar S. A survey on face recognition systems. arXiv:2201.02991. 2022.
5. Yu Z, Qin Y, Li X, Zhao C, Lei Z, Zhao G. Deep learning for face anti-spoofing: a survey. IEEE Trans Pattern Anal Mach Intell. 2022;45(5):5609–31. doi:10.1109/tpami.2022.3215850.
6. Arora S, Bhatia MPS, Mittal V. A robust framework for spoofing detection in faces using deep learning. Vis Comput. 2022;38(7):2461–72. doi:10.1007/s00371-021-02123-4.
7. Huang PK, Chiang CH, Chen TH, Chong JX, Liu TL, Hsu CT. One-class face anti-spoofing via spoof cue map-guided feature learning. In: 2024 IEEE/CVF Conference on Computer Vision and Pattern Recognition (CVPR); 2024 Jun 16–22: Seattle, WA, USA: IEEE. p. 277–86 202410.1109/CVPR52733.2024.00034.
8. Huang PK, Chong JX, Chiang CH, Chen TH, Liu TL, Hsu CT. SLIP: spoof-aware one-class face anti-spoofing with language image pretraining. Proc AAAI Conf Artif Intell. 2025;39(4):3697–706. doi:10.1609/aaai.v39i4.32385.
9. Xing H, Tan SY, Qamar F, Jiao Y. Face anti-spoofing based on deep learning: a comprehensive survey. Appl Sci. 2025;15(12):6891. doi:10.3390/app15126891.
10. Huang PK, Chong JX, Hsu MT, Hsu FY, Chiang CH, Chen TH, et al. A survey on deep learning-based face anti-spoofing. APSIPA Trans Signal Inf Process. 2024;13(1):1–33. doi:10.1561/116.20240053.
11. Viquerat J, Duvigneau R, Meliga P, Kuhnle A, Hachem E. Policy-based optimization: single-step policy gradient method seen as an evolution strategy. Neural Comput Appl. 2023;35(1):449–67. doi:10.1007/s00521-022-07779-0.
12. Le N, Rathour VS, Yamazaki K, Luu K, Savvides M. Deep reinforcement learning in computer vision: a comprehensive survey. Artif Intell Rev. 2022;55(4):2733–819. doi:10.1007/s10462-021-10061-9.
13. Zhang K, Sun M, Han TX, Yuan X, Guo L, Liu T. Residual networks of residual networks: multilevel residual networks. IEEE Trans Circuits Syst Video Technol. 2018;28(6):1303–14. doi:10.1109/TCSVT.2017.2654543.
14. Hu J, Shen L, Sun G. Squeeze-and-excitation networks. In: Proceedings of the IEEE Conference on Computer Vision and Pattern Recognition; 2018 Jun 18–22; 2018; Salt Lake City, UT, USA. p. 7132–41.
15. Shen T, Huang Y, Tong Z. FaceBagNet: bag-of-local-features model for multi-modal face anti-spoofing. In: 2019 IEEE/CVF Conference on Computer Vision and Pattern Recognition Workshops (CVPRW); 2019 Jun 16–17; Long Beach, CA, USA: IEEE. p. 1611–6. doi:10.1109/cvprw.2019.00203.
16. Parkin A, Grinchuk O. Recognizing multi-modal face spoofing with face recognition networks. In: 2019 IEEE/CVF Conference on Computer Vision and Pattern Recognition Workshops (CVPRW); 2019 Jun 16–17; Long Beach, CA, USA: IEEE. p. 1617–23. doi:10.1109/cvprw.2019.00204.

17. Chen X, Xu S, Ji Q, Cao S. A dataset and benchmark towards multi-modal face anti-spoofing under surveillance scenarios. IEEE Access. 2021;9:28140–55. doi:10.1109/access.2021.3052728.
18. Zheng T, Li B, Wu S, Wan B, Mu G, Liu S, et al. MFAE: masked frequency autoencoders for domain generalization face anti-spoofing. IEEE Trans Inf Forensics Secur. 2024;19:4058–69. doi:10.1109/TIFS.2024.3371266.
19. Kong C, Zheng K, Liu Y, Wang S, Rocha A, Li H. M^3FAS: an accurate and robust MultiModal mobile face anti-spoofing system. IEEE Trans Dependable Secure Comput. 2024;21(6):5650–66. doi:10.1109/TDSC.2024.3381598.
20. Nathan S, Beham MP, Nagaraj A, Roomi SMM. Multiattention-net: a novel approach to face anti-spoofing with modified squeezed residual blocks. In: 2024 IEEE/CVF Conference on Computer Vision and Pattern Recognition Workshops (CVPRW); 2024 Jun 17–18; Seattle, WA, USA: IEEE. p. 1013–20. doi:10.1109/CVPRW63382.2024.00107.
21. Fatemifar S, Awais M, Akbari A, Kittler J. Particle swarm and pattern search optimisation of an ensemble of face anomaly detectors. In: 2021 IEEE International Conference on Image Processing (ICIP); 2021 Sep 19–22; Anchorage, AK, USA: IEEE; 2021. p. 3622–6. doi:10.1109/ICIP42928.2021.9506251.
22. Chingovska I, Anjos A, Marcel S. On the effectiveness of local binary patterns in face anti-spoofing. In: Proceedings of the 2012 BIOSIG-Proceedings of the International Conference of Biometrics Special Interest Group (BIOSIG); 2012 Sep 6–7; Darmstadt, Germany. p. 1–7.
23. Costa-Pazo A, Bhattacharjee S, Vazquez-Fernandez E, Marcel S. The replay-mobile face presentation-attack database. In: 2016 International Conference of the Biometrics Special Interest Group (BIOSIG); 2016 Sep 21–23; Darmstadt, Germany: IEEE; 2016. p. 1–7.
24. Li H, Li W, Cao H, Wang S, Huang F, Kot AC. Unsupervised domain adaptation for face anti-spoofing. IEEE Trans Inf Forensics Secur. 2018;13(7):1794–809. doi:10.1109/TIFS.2018.2801312.
25. Sedik A, Faragallah OS, El-sayed HS, El-Banby GM, El-Samie FEA, Khalaf AAM, et al. An efficient cybersecurity framework for facial video forensics detection based on multimodal deep learning. Neural Comput Appl. 2022;34(2):1251–68. doi:10.1007/s00521-021-06416-6.
26. Smith DF, Wiliem A, Lovell BC. Face recognition on consumer devices: reflections on replay attacks. IEEE Trans Inf Forensics Secur. 2015;10(4):736–45. doi:10.1109/TIFS.2015.2398819.
27. Kong Y, Li X, Hao G, Liu C. Face anti-spoofing method based on residual network with channel attention mechanism. Electronics. 2022;11(19):3056. doi:10.3390/electronics11193056.
28. Huang R, Wang X. Face anti-spoofing using feature distilling and global attention learning. Pattern Recognit. 2023;135(10):109147. doi:10.1016/j.patcog.2022.109147.
29. Liu Y, Jourabloo A, Liu X. Learning deep models for face anti-spoofing: binary or auxiliary supervision. In: 2018 IEEE/CVF Conference on Computer Vision and Pattern Recognition; 2018 Jun 18–23; 2018; Salt Lake City, UT, USA: IEEE. p. 389–98. doi:10.1109/CVPR.2018.00048.
30. Boulkenafet Z, Komulainen J, Li L, Feng X, Hadid A. OULU-NPU: a mobile face presentation attack database with real-world variations. In: 2017 12th IEEE International Conference on Automatic Face & Gesture Recognition (FG 2017); 2017 May 30–Jun 3; Washington, DC, USA. IEEE; 2017. p. 612–8. doi:10.1109/FG.2017.77.
31. Zhang Z, Yan J, Liu S, Lei Z, Yi D, Li SZ. A face antispoofing database with diverse attacks. In: 2012 5th IAPR International Conference on Biometrics (ICB); 2012 Mar 29–Apr 1; New Delhi, India: IEEE; 2012. p. 26–31. doi:10.1109/ICB.2012.6199754.
32. Wen D, Han H, Jain AK. Face spoof detection with image distortion analysis. IEEE Trans Inf Forensics Secur. 2015;10(4):746–61. doi:10.1109/TIFS.2015.2400395.
33. Xue H, Ma J, Guo X. A hierarchical multi-modal cross-attention model for face anti-spoofing. J Vis Commun Image Represent. 2023;97(8):103969. doi:10.1016/j.jvcir.2023.103969.
34. Zhang S, Liu A, Wan J, Liang Y, Guo G, Escalera S, et al. CASIA-SURF: a large-scale multi-modal benchmark for face anti-spoofing. IEEE Trans Biom Behav Identity Sci. 2020;2(2):182–93. doi:10.1109/TBIOM.2020.2973001.
35. Liu A, Tan Z, Wan J, Escalera S, Guo G, Li SZ. CASIA-SURF CeFA: a benchmark for multi-modal cross-ethnicity face anti-spoofing. In: 2021 IEEE Winter Conference on Applications of Computer Vision (WACV); 2021 Jan 3–8; Waikoloa, HI, USA: IEEE; 2021. p. 1178–86. doi:10.1109/WACV48630.2021.00122.

36. George A, Mostaani Z, Geissenbuhler D, Nikisins O, Anjos A, Marcel S. Biometric face presentation attack detection with multi-channel convolutional neural network. IEEE Trans Inf Forensics Secur. 2019;15:42–55. doi:10.1109/TIFS.2019.2916652.
37. Yu Z, Cai R, Cui Y, Liu X, Hu Y, Kot AC. Rethinking vision transformer and masked autoencoder in multimodal face anti-spoofing. Int J Comput Vis. 2024;132(11):5217–38. doi:10.1007/s11263-024-02055-1.
38. Gautam V, Kaur G, Malik M, Pawar A, Singh A, Kant Singh K, et al. FFDL: feature fusion-based deep learning method utilizing federated learning for forged face detection. IEEE Access. 2024;13(2):5366–79. doi:10.1109/access.2024.3523257.
39. Yang X, Liu W, Liu W, Tao D. A survey on canonical correlation analysis. IEEE Trans Knowl Data Eng. 2021;33(6):2349–68. doi:10.1109/TKDE.2019.2958342.
40. Rossler A, Cozzolino D, Verdoliva L, Riess C, Thies J, Niessner M. FaceForensics++: learning to detect manipulated facial images. In: 2019 IEEE/CVF International Conference on Computer Vision (ICCV); 2019 Oct 27–Nov 2; Seoul, Republic of Korea. IEEE; 2019. p. 1–11. doi:10.1109/iccv.2019.00009.
41. Jiang L, Li R, Wu W, Qian C, Loy CC. DeeperForensics-1.0: a large-scale dataset for real-world face forgery detection. In: 2020 IEEE/CVF Conference on Computer Vision and Pattern Recognition (CVPR); 2020 Jun 13–19; Seattle, WA, USA: IEEE; 2020. p.13–19. doi:10.1109/cvpr42600.2020.00296.
42. Zi B, Chang M, Chen J, Ma X, Jiang YG. WildDeepfake: a challenging real-world dataset for deepfake detection. In: Proceedings of the 28th ACM International Conference on Multimedia. Seattle, WA, USA: ACM; 2020. p. 2382–90. doi:10.1145/3394171.3413769.
43. Li N, Weng Z, Liu F, Li Z, Wang W. Dual-path adaptive channel attention network based on feature constraints for face anti-spoofing. IEEE Access. 2025;13:22855–67. doi:10.1109/access.2025.3534906.
44. Chen G, Xie W, Lin D, Liu Y, Wang M. mmFAS: multimodal face anti-spoofing using multi-level alignment and switch-attention fusion. Proc AAAI Conf Artif Intell. 2025;39(1):58–66. doi:10.1609/aaai.v39i1.31980.
45. Heusch G, George A, Geissbühler D, Mostaani Z, Marcel S. Deep models and shortwave infrared information to detect face presentation attacks. IEEE Trans Biom Behav Identity Sci. 2020;2(4):399–409. doi:10.1109/TBIOM.2020.3010312.
46. Kumar Y, Ilin A, Salo H, Kulathinal S, Leinonen MK, Marttinen P. Self-supervised forecasting in electronic health records with attention-free models. IEEE Trans Artif Intell. 2024;5(8):3926–38. doi:10.36227/techrxiv.23911365.v1.
47. Ho J, Kalchbrenner N, Weissenborn D, Salimans T. Axial attention in multidimensional transformers. arXiv:1912.12180. 2019.
48. Li J, Wang X, Tu Z, Lyu MR. On the diversity of multi-head attention. Neurocomputing. 2021;454:14–24. doi:10.1016/j.neucom.2021.04.038.
49. Zhao X, Guo J, Zhang Y, Wu Y. Asymmetric bidirectional fusion network for remote sensing pansharpening. IEEE Trans Geosci Remote Sens. 2023;61:5404816. doi:10.1109/TGRS.2023.3296510.
50. Wang T, Yang L. Beetle swarm optimization algorithm: theory and application. arXiv:1808.00206. 2018.
51. Khade S, Gite S, Pradhan B. Iris liveness detection using multiple deep convolution networks. Big Data Cogn Comput. 2022;6(2):67. doi:10.3390/bdcc6020067.
52. Krasnodębska K, Goch W, Uhl JH, Verstegen JA, Pesaresi M. Advancing precision, recall, F-score, and jaccard index: an approach for continuous, ratio-scale measurements. Environ Model Softw. 2025;193:106614. doi:10.1016/j.envsoft.2025.106614.